Establishing the hydrological controls on water surface area variations in oxbow lakes

Joshua Ahmed[1*]

[1]*Energy and Environment Institute, University of Hull, Hull, HU6 7RX*

*geomorphicjosh@gmail.com

Abstract

Oxbow lakes are iconic fluvial landforms found in the floodplains of meandering rivers around the world. Their formation is associated with meander cutoff, a process that excises sections of river channel to optimise the downstream transmission of water and sediment. After termination, sedimentary plugs form at either end of the abandoned channel to isolate it from the mainstem. Overbank floods and conveyance through tie channels maintains some hydrological connectivity, but lakes are generally considered to passively infill until they become terrrestrialised. Here, a suite of 64 lakes across two meandering rivers in the Bolivian Amazon are used to demonstrate the hydrological dynamism of oxbow lakes after cutoff by quantifying interannual variations in lake water surface area (WSA) and the mechanisms controlling them. The results suggest that WSA variations are controlled by proximity to the active channel, with the magnitude of these variations being set by mechanisms of connectivity. Lakes connected by tie channels experienced WSA changes up to 3.9 times larger than lakes with no visible connection mechanisms. Incursion lakes displayed similar WSA changes to those with tie channels, while isolated lakes were found furthest from the mainstem and had the smallest range of WSAs. Chute-lakes experienced a wider range of WSAs and were more strongly controlled by mainstem proximity than neck-lakes. An understanding of the processes governing oxbow lake hydrodynamics is important for

26 forecasting nutrient and contaminant fluxes as well as the sensitivity of riparian wetlands to

27 changes in catchment hydrology associated with climate change and flow modification.

28 **Keywords**

29 Oxbow lakes, wetlands, meandering, cutoff, connectivity

30

31 **1. Introduction**

32 Oxbow lakes are widespread geomorphic features found along the floodplains of meandering

33 rivers around the world. These specialist ecotones serve as habitats for a range of aquatic

34 and terrestrial species, while also forming reservoirs for sediments, nutrients, and

35 contaminants (Constantine *et al.*, 2010a; Thomas *et al.*, 2021; Nifong *et al.*, 2022). To

36 effectively safeguard the future functioning of oxbow lakes and conserve the suite of

37 ecosystem services they provide, it is essential to understand how lakes evolve over different

38 timescales and classify the mechanisms responsible for their evolution.

39 Lakes are formed through the process of meander cutoff – where bends are terminated from

40 active service in favour of shorter, steeper down-valley flow routes (Allen, 1965; Constantine

41 *et al.*, 2010b). Once terminated, bends undergo four stages of evolution, culminating in

42 terrestrialisation – where the abandoned section no longer conveys water (Gagliano and

43 Howard, 1984). This evolutionary process occurs over timescales of decades to centuries and

44 is principally controlled by sediment deposition within the lakes (Gagliano and Howard, 1984;

45 Citterio and Piégay, 2009; Constantine *et al.*, 2010b). Over this period of infilling, lakes are

46 exposed to exogenous water sources from precipitation, episodic and seasonal flooding, and

47 groundwater seepage (Rowland *et al.*, 2009; Guo *et al.*, 2023; Bagheri *et al.*, 2024); these

48 additions, paired with evaporative and drainage based losses, permit fluctuations in lake water

49 volume through time, which changes the hydrochemical characteristics of the lakes, and

50 influences the trophic structure within them (Obolewski *et al.,* 2009; Kufel and Leśniczuk,

51 2014; Scarabotti *et al.*, 2017; Saha *et al.*, 2022). Identifying the mechanisms responsible for

52 changes in lake water volume and the timescales over they occur is critical for establishing

how these lakes may respond to future changes in catchment hydrology driven by climate change and human modification (Jaeger *et al.*, 2014; Anderson *et al.*, 2018; Nielsen *et al.*, 2020; Arantes *et al.*, 2022).

Actively migrating meandering rivers replace aging floodplain deposits with younger fertile sediments and create rich wetland habitat possessing topographic and ecological diversity (Sioli, 1975; Lauer and Parker, 2008; Constantine *et al.*, 2014; Lewin and Ashworth, 2014). Over time, the progressive increase in channel sinuosity and decrease in channel slope enhances the channel's susceptibility to cutoff (Constantine and Dunne, 2008). Meander cutoff can occur by two distinct mechanisms: neck cutoff – where two meander bends converge – and chute cutoff, where a bend-scale avulsion occurs, bypassing the original meander bend (**Fig. 1**) (Lewis and Lewin, 1983; Hooke, 1995). Chute channel formation occurs in several ways and is usually driven by the site specific characteristics of the floodplain and hydrograph. For example, on the Sacramento River (USA), Constantine et al. (2010b) described chute channel initiation through the downstream extension of embayments that formed near regions of maximum channel curvature, due to overbank spilling during floods. Several authors reported flood-triggered headcut extension over the floodplain separating multiple meander bends, some of which were caused by in-channel blockages (Gay *et al.*, 1998). Floodplain relief also plays a pivotal role in the development of chute channels, particularly where overbank flows exploit topographic lows to channelize flow and form a breach (Zinger *et al.*, 2011; Lewis *et al.*, 2020; Schwendel and Cooper, 2021).

The oxbow lakes produced by neck and chute cutoffs have considerably different evolutionary pathways due to variations in flow partitioning between the new and abandoned channels, which changes the rate of infilling and calibre of material being sequestered in the abandoned channel (Constantine *et al.*, 2010a; Dieras, 2013; Richards *et al.*, 2022). Typically, within the first decade of cutoff formation, coarse-grained sediment plugs form at the entrance and exit of the abandoned channel to isolate it from the mainstem (Gagliano and Howard, 1984; Hooke, 1995). This process is driven by the divergence angle between the new and abandoned

80 channel segments, with higher angles promoting accelerated plug formation due to a wider

81 region of flow separation (Bridge *et al.*, 1986; Constantine *et al.*, 2010a). Higher angles tend

82 to be associated with neck cutoffs, while chutes have lower angles allowing the abandoned

83 channel to continue transmitting flow and sediment, which in some cases, allows them to

84 remain hydromorphologically active long after cutoff was first initiated (Grenfell *et al.*, 2012).

85 Similarly, recent field observations revealed that neck cutoffs with complex curvatures can

86 also successfully advect sediment into the abandoned channel and away from the entrance

87 and exit, thus precluding plug development and extending the time taken for the lake to

88 become isolated from the mainstem (Richards and Konsoer, 2020; Turnipseed *et al.*, 2021).

89 Once the abandoned channel has been isolated and becomes lacustrine, interactions with the

90 mainstem are limited to those made during overbank floods or through tie channels and

91 incursion (Gagliano and Howard, 1984; Rowland *et al.*, 2009). Evidence for these interactions

92 is clearly illustrated from remote sensing data where abrupt turbidity gradients form as

93 sediment-laden river water enters the lakes during floods (**Fig. 2**); although these observations

94 may be more nuanced in rivers with lower sediment yields. These hydrological interactions

95 are important for the long-term evolution of lake physiochemistry, contaminant and organic

96 matter storage, and the wider provision of ecosystem services to riverine communities.

97 Despite this, a quantitative appraisal of lake evolution through time remains absent from the

98 literature particularly with respect to shorter-term variations, which will be more sensitive to

99 localised hydrological phenomena (e.g., flooding).

100 The extensive Landsat multispectral remote sensing record (1984-present) provides the

101 opportunity to monitor annual variations in oxbow lake water surface area (WSA) and forms a

102 tangible method for assessing the hydrological dynamism over annual and interannual

103 timescales. This study, for the first time, quantifies interannual WSA variations for 64 oxbow

104 lakes in the south-west Bolivian Amazon Basin and answers three core research objectives:

105 1) How does the WSA of oxbow lakes vary through time?

106 2) What are the key mechanisms driving WSA change in oxbow lakes?

107   3) Does lake type (i.e., neck or chute) affect WSA variability?

Materials and Methods

109   1.1 Study site

110   The study was focused on two highly dynamic meandering rivers in the south-west Bolivian

111   Amazon Basin (**Fig. 3**). The Río Beni and Río Mamoré display some of the highest rates of

112   meander migration (10-22 metres per year; *m yr^{-1}*) and cutoff formation in the Amazon

113   (Constantine *et al.*, 2014). Over the 38 year period between 1984 and 2022, the Beni and

114   Mamoré rivers produced 28 and 36 cutoffs, respectively, adding to the already extensive

115   population of oxbow lakes in their floodplains (162 and 257 for the Beni and Mamoré). These

116   rivers are ideal candidates to explore hydrological behaviour since they experience large water

117   level fluctuations (> 10 m) between the wet and dry seasons and are relatively unimpacted by

118   anthropogenic disturbance (e.g., dams or channel control structures), thus allowing natural

119   channel-floodplain interactions to be observed (Finer and Jenkins, 2012; Latrubesse *et al.*,

120   2017; Ahmed *et al.*, 2019).

121   The Beni drains an area of 67,500 km^2 of the northern Andes before emerging from the

122   Andean foothills and transitioning to a rapidly migrating meandering pattern in response to the

123   abrupt decrease in longitudinal gradient and increase in valley width (Guyot *et al.*, 1996;

124   Gautier *et al.*, 2007). Measurements of sediment flux at Rurrenabaque – where the river

125   emerges from the Andes – indicate an annual suspended sediment flux of 212 megatons per

126   year (Mt yr^{-1}), most of which is captured by the downstream channel-floodplain system (Guyot

127   *et al.*, 1996). The Mamoré is *ca.* 270 km south east of the Beni and forms at the confluence of

128   the Rio Ichilo and Rio Chimore that drains ~7600 km^2 of the east Andean Cordillera, yielding

129   an estimated suspended sediment flux of 13 Mt yr^{-1} (Guyot *et al.*, 1996; Constantine *et al.*,

130   2014). However, this sediment flux abruptly increases at the confluence with the Rio Grande

131   100 km downstream, which delivers an additional 82 Mt yr^{-1} from a 23,700 km^2 area of the

132   eastern Andes (Guyot *et al.*, 1996). Similar to the Beni, the Mamoré deposits and stores a

large amount of this sediment within the lowland channel-floodplain system (Constantine *et al.*, 2014).

Separating the two rivers is a vast floodplain savannah interspersed with evergreen forest spanning around 170,000 km^2 – the Llanos de Moxos (Hamilton *et al.*, 2004). The savannah region becomes seasonally, and in places, permanently, inundated as discharges on the Beni and Mamoré reach their maximum in austral summer (January – March) in response to several months of heavy rainfall, with the highest rates concentrated near the Andes (Killeen *et al.*, 2007; Bookhagen and Strecker, 2008). As water disperses across the Llanos de Moxos depths do not typically exceed 1 m, although the total floodwater extent is estimated to cover almost the whole region (Hamilton *et al.*, 2004; Fleischmann *et al.*, 2022).

Precipitation patterns are altered during El Niño-Southern Oscillation (ENSO) years, with El Niño years typically delivering less than average rainfall, and La Niña years delivering more than average to these Bolivian catchments (Aalto *et al.*, 2003; Bookhagen and Strecker, 2010; Espinoza *et al.*, 2013). South Atlantic sea surface temperature anomalies are also responsible for enhancing precipitation over south-western Amazonia and can further intensify rainfall patterns associated with La Niña conditions (Espinoza *et al.*, 2013, 2014). During these years, the extent and residence time of floodwater inundation increases, thus impacting the hydrodynamic behaviour of rivers and floodplain wetlands (Bourrel *et al.*, 2009; Ovando *et al.*, 2016).

The distribution of oxbow lakes varies across each basin as a function of channel mobility: lakes that were excised near the start of the record could now be long distances away from the active channel, while newly cutoff lakes could be closer. However, this is not always the case, since both rivers migrate rapidly across their floodplains, meaning the active channel could now have returned to the site of a former cutoff. The diversity of lakes allows for the controls on hydrological behaviour to be investigated between and within each river system.

1.2 Remote sensing

159   Recently formed (1984-2022) meander cutoffs were identified and classified as either neck or

160   chute from multispectral timelapse imagery for the Beni and Mamoré using the USGS and

161   NASA Landsat imagery archive and processed through Google Earth Engine (Gorelick *et al.*,

162   2017). Water surface areas were computed for each lake using the modified Normalised

163   Difference Water Index (mNDWI), which exploits the ratio of light reflected and absorbed in

164   the green and near infrared portions of the electromagnetic spectrum (as captured by Landsat)

165   (Xu, 2006). Each river was comprised of two image scenes, thus dividing the reach into an

166   upper and lower section centred on B-10 and M-20 for the Beni and Mamoré, respectively.

167   These sub-reaches were only used during compilation of the imagery.

168   To optimise the extraction of WSAs, images were selected between June and October each

169   year, when cloud cover was at a minimum. These months are representative of a descending

170   flood wave following the wet season meaning WSAs are likely conservative compared to those

171   captured between January and March when cloud coverage is high. In some cases, where

172   localised cloud coverage prevented lake observations from being made, an alternative image

173   was sought from a different date within the observation window. In rare cases where cloud-

174   free images were unavailable, an extended observation window (May-November) was used

175   to obtain a cloud-free image. This process was performed for each year on record until image

176   resolution (30 m/pixel) precluded wetted pixel detection or the lake was completely

177   terrestrialised. WSA measurements were normalised by the year 1 centreline lake length,

178   since longer lakes will have larger aerial extents. Each WSA was stacked and used to compute

179   the percentage relative difference between years (**Fig. 4**).

180   Channel centrelines were created using a semi-automated Python-based workflow from

181   Normalised Difference Vegetation Index (NDVI) imagery using Google Earth Engine. The

182   NDVI was used to extract the bankfull channel boundary – demarcated by an abrupt transition

183   from vegetated to unvegetated pixels – and edited to remove hydrologically connected

184   elements (e.g., tie channels and proximal lakes). The filtered channel boundaries were then

185   used to create centrelines for each year on record (Ahmed *et al.*, 2019; Sylvester *et al.*, 2021).

186   Proximity measurements were made by measuring the closest orthogonal distance between

187   channel centreline and WSA (**Fig. 5a**) and used as a surrogate for river discharge, which was

188   unavailable for the correct duration and locations in the present study. This method does not

189   constrain closest distance measurements to the entrance and exit of the lakes; therefore, the

190   closest orthogonal distance could be over the floodplain and through the rainforest. This is

191   feasible since overbank flows are governed by the prevailing water level in the channel, which

192   once greater than the elevation of the river bank, will flow across the shallow sloping floodplain

193   surface to the lakes, where topography and floodplain roughness permits (Aalto *et al.*, 2003;

194   Ovando *et al.*, 2018).

195   Monthly rainfall was computed from the daily Climate Hazards Group InfraRed Precipitation

196   with Station (CHIRPS) dataset and summed over each water year (October – September),

197   which aligns with the same period used to derive the WSA and centreline datasets and follows

198   the timing of seasonal rainfall. A rainfall record was produced for each lake from discrete points

199   situated within a 5.5 km^2 resolution grid (one for each lake) (**Fig. 5b**). Total seasonal rainfall

200   was computed as the total monthly rainfall between October and March, which corresponds

201   to the wet season in Bolivia. ENSO years were classified according the National Oceanic and

202   Atmospheric Administration (NOAA) southern oscillation index (SOI), which is computed as

203   the standardised index of sea level pressure difference between Tahiti and Darwin (NOAA,

204   2024).

205   Three broad connectivity mechanisms were adopted to classify each lake: isolation, incursion,

206   and tie channel (**Fig. 6**). Isolation was assigned to lakes where there was no obvious indication

207   of hydrological connectivity from the imagery; incursion was assigned where the active

208   channel breached the year one lake WSA boundary; and, tie channel was used where clear

209   evidence of tie channels connecting the mainstem – or adjacent river channels – to the lakes

210   were present. Each lake was assigned a category after visually inspecting the corresponding

211   Landsat images over the full lifetime of the lakes. Indeed, this method precludes the

212   identification of features finer than the image resolution (30 m); however, most features

213   exceeded single pixel values in scale, thus permitting accurate classification. Where lakes

214 transitioned from one category to another (e.g., where a tie channel connected lake become

215 isolated due to infill of the tie channel), the year in which the change occurred was classified

216 accordingly. Where lakes were characterised by incursion, the proximity value became 0 m,

217 indicative of the centreline breaching the lake boundary. Uncertainty around these

218 measurements is approximately 0.5 channel widths (Beni: 210 m; Mamoré: 155 m, based on

219 30 measurements of channel width from straight sections of each river), since distance from

220 the centreline was used to measure proximity, rather than the wetted channel boundary.

Results

222 WSA variations on both the Mamoré and Beni were significant and followed multiple

223 trajectories over time. Long-term trends (i.e., from inception to present day) were mixed: 25%

224 of lakes (16) increased in size by between +7% and +142% of their original WSA, while the

225 majority of lakes (48) decreased in size by up to 100% of their starting WSA (**Fig. 7**). However,

226 when looking at WSA changes over interannual timescales, the behaviour became more

227 complex. All of the lakes, for at least some portion of their lifetime, oscillated from positive to

228 negative WSA change between years. Changes within single years varied, on average, by up

229 to -100% or +281% of the previous year's WSA, exceeding changes observed when only

230 considering areas measured at the start and end of the WSA record (black line; **Fig. 8**).

231 Average annual changes across all of the lakes were -17% to +24% with no observed patterns

232 of WSA change with distance downstream or with lake age (**Fig. 9**). Breaks in WSA trajectories

233 at 2002 and 2012 were indicative of missing images from the temporal record (**Fig. 7**).

234 Examining the variability in WSAs across the two reaches demonstrated that some lakes had

235 tightly constrained changes over their lifespan, while others were more variable (**Fig. 9**). In

236 general, lakes with longer temporal records experienced larger variations in WSA (*Kendall τ =*

237 *0.31; Spearman's ρ = 0.46; p<0.001*) (**Fig. S1**). However, several younger oxbow lakes (≤ 6

238 years old) on both the Mamoré and Beni experienced large variations in WSA (e.g., B-23, B25,

239 M-17), suggesting that age did not have a first order control.

240   Lake formation mechanism (i.e., neck versus chute) appeared to influence annual WSA

241   changes: those associated with necks showed more limited change compared to those

242   associated with chutes (*Kruskal Wallis (KW): p<<0.0001*) (**Fig. 10**), but both had similar long-

243   term WSA reductions (necks: -24% and chutes: -30%). Over interannual timescales, WSA

244   changes for chute lakes ranged from -95% to +281%, while neck-derived lakes experienced

245   smaller maximum annual increases in WSA (+188%), but a similar magnitude of decrease (-

246   92%). Average positive and negative WSA changes for necks were +15% and -14%,

247   respectively, while the average WSA changes for chutes were +43% and -23%, indicating

248   larger interannual variability for chute-derived lakes. The majority of lakes (39 of 64)

249   experienced interannual WSA changes that exceeded the total relative area change measured

250   between the start and end of the record. Instances of interannual WSA changes that exceeded

251   the long-term change were not associated with a particular type of cutoff lake; both neck- and

252   chute-derived lakes were equally as likely to exceed the long-term average change.

253   Evaluating the lake populations in full revealed that lakes from any given year did not

254   contemporaneously increase or decrease in WSA. For the majority of years (29), lake

255   populations were comprised of both positive and negative WSA changes (**Fig. 11**). These

256   positive and negative changes did not favour particular lake types (i.e., chute or neck), with

257   no statistically significant differences observed between the positive and negative changes for

258   chute and neck lakes in any given year (*KW: p>0.67*) (**Fig. S2**). To test whether lakes

259   responded contemporaneously when perturbed by large-scale climatic phenomena, ENSO

260   indices were mapped against the proportion of lakes that increased or decreased in WSA.

261   Some coherence was observed in positive (El Niño) and negative (La Niña) years, where the

262   majority of lakes decreased and increased in size, respectively (**Fig. S3**), but there were still

263   anomalous years where WSAs were expected to decrease in response to El Niño (e.g., 1992),

264   but increased, or vice versa in La Niña years (e.g., 2022).

265   Total seasonal rainfall was used as a surrogate for total annual rainfall since the majority of

266   precipitation falls between October and March in this region of Amazonia ($\tau = 0.73$;

267   *Spearman's ρ = 0.90; p<<0.001)* (**Fig. 12a**). WSAs were weakly correlated with respect to total

268   seasonal rainfall, with both rainfall minima and maxima invoking similar sizes of lake (*τ = 0.063;*

269   *ρ = 0.094; p<0.003*) (**Fig. 12b**). Partitioning WSAs by cutoff type revealed a similarly weak

270   total precipitation control on WSA for neck-derived lakes (*τ = 0.047; ρ = 0.070; p<<0.06*), but

271   a stronger positive correlation (*τ = 0.17; ρ = 0.25; p<<0.001*) for chute-derived lakes.

272   Changes in WSA were very weakly negatively correlated with proximity to the mainstem (**Fig.**

273   **13a**). However, when testing the statistical robustness of these correlations, only the Kendall's

274   Tau test found the relationship to be significant (*τ = -0.049; p<0.03).* To investigate the

275   relationship further, the data were partitioned by cutoff type: this revealed that WSA changes

276   in chute-derived lakes were more strongly controlled by proximity to the mainstem (*τ = -0.11;*

277   *Spearman's ρ = -0.15; p<<0.02)* than neck-derived lakes, which were not statistically

278   correlated (p>0.33). Lakes from both populations were most receptive to changes in WSA

279   when situated within 1 km of the mainstem; however, with increasing distance from the active

280   channel, WSAs diminished. Mainstem proximity was observed to exert greater control on

281   chute lakes in the distal floodplain (>4 km away), while neck-derived lakes stopped being

282   receptive to mainstem proximity once distances exceeded 2.5 km (**Fig. 13b**).

283   To develop a clearer understanding of how channel proximity affects lake WSA, the temporal

284   variability was removed by computing the mean channel proximity and standard deviation of

285   WSAs for each lake over their full lifetime (**Fig 13c**). This demonstrated a clearer control of

286   channel proximity on lake WSA, particularly when lakes were within 400 m of the mainstem.

287   Lakes situated greater than 400 m from the mainstem had WSAs around 1.7 times smaller

288   than the maximum values observed for lakes within 400 m of the mainstem, although the

289   minimum standard deviation of WSAs were comparable (within 7%).

290   Examining WSA variations by lake connection style reveals further insights to the mechanistic

291   controls on the observed variations. The majority of lakes (68%) were connected to the

292   mainstem by tie channels (n=551), while those characterised by incursion represented around

293   27% (n=219), and the remaining lakes (n=39) were isolated from mainstem or other visible

294   hydrological connections (**Fig. 14**). Lakes connected by tie channels showed the largest range

295   of WSAs (*Tie channels = 0.40; Isolated = 0.14; Incursion = 0.30 km^2 km^{-1}*) and had the highest

296   average areas (*Tie channels = 0.15; Isolated = 0.042; Incursion = 0.081 km^2 km^{-1}*) of the three

297   groups, while isolated lakes had the smallest range. Lakes that experienced mainstem

298   incursion displayed a wide range of WSAs and average areas that exceeded isolated lakes,

299   but were less than those connected by tie channels. The minimum WSA for each group was

300   similar, but each class was statistically distinct (*KW: p<0.001*).

301   The proximity of lakes with tie channels varies from 0 – 4178 m, with an average distance of

302   490 m and the 90th-percentile (P_{90}) of the distribution at 899 m from the mainstem. Incursion

303   based lakes have proximities ranging from 0 to 2205 m and a P_{90} of 1.82 km. The

304   measurements were inclusive of uncertainties introduced by measuring distances from the

305   centreline (~0.5 channel widths) to the year 1 lake boundary, and instances of multiple cutoff,

306   where incursion has already occurred and a second termination causes the channel to retreat

307   further away from the initial lake (e.g., M-15). The proximity of isolated lakes from the

308   mainstem was between 128 and 4136 m, with P_{90} being 3.93 km. Realistically, proximity

309   measurements of 0 m are bound by a 30 m uncertainty envelope, which corresponds to the

310   resolution of the imagery.

311   **Discussion**

312   Oxbow lakes are considered to be relatively passive lentic environments once cutoff and plug

313   formation has occurred, slowly infilling with sediment delivered by overbank floods or through

314   connecting channels until they are fully terrestrialised (Gagliano and Howard, 1984; Rowland

315   *et al.*, 2005). This notion is supported by long-term WSA measurements for the majority (75%)

316   of lakes on the Beni and Mamoré, which showed an average decrease of ~-45% (**Fig. 7**).

317   However, estimates of WSA change, and how they relate to the lake's morphological

318   evolution, should be made with caution since the observation window over which changes are

319   measured could produce multiple divergent patterns of evolution for a single lake through time.

320   For example, most lakes experienced oscillations in WSA from positive to negative (or vice

321 versa) over the course of the temporal record, which could cause false interpretations of a

322 lake's long-term evolution if the window only captured a single phase of change in time. This

323 is particularly important when making comparisons of terrestrialisation timescales for lakes

324 within or between catchments. Periods of negative change – that is, where WSA decreases

325 from the previous timestep – may be incorrectly interpreted as periods of infilling, where a

326 WSA reduction would also be expected. This would present challenges when attempting to

327 reconcile remote sensing observations with those from the stratigraphic record, particularly

328 where a subsequent increase in WSA may be falsely interpreted as an erosional phase (Dieras

329 *et al.*, 2013; Richards *et al.*, 2022).

330 Despite lakes being spatially co-located within each catchment, many did not show

331 contemporaneous positive or negative changes in WSA in the same year (**Fig. 11**). Indeed,

332 some of this variability could be explained by differences in acquisition date, where images

333 acquired closer to the wet season termination would have larger WSAs than those acquired

334 towards the end of the dry season, after several months of evaporation and return flow from

335 lakes to the mainstem. However, when reviewing lake measurements taken from the same

336 images, this pattern of diverging positive and negative WSA change persists, indicating that

337 the behaviour must be controlled by an alternative mechanism. Some coherence was found

338 between lakes in years where regional rainfall patterns were altered by ENSO, but lake

339 behaviour was not consistent across all events (**Fig. S3**). Indeed, timing and severity of these

340 climatic phenomena can trigger differences in lake response (Marengo and Espinoza, 2016),

341 but should be relatively consistent across the watershed, suggesting an alternative

342 mechanistic control on lake WSAs.

343 The simplest explanation for changes in WSA is through mechanisms that directly influence

344 the local water balance of the lake. Hydrological inputs are limited to those from rainwater, the

345 active channel, proximal floodplain wetlands, or groundwater (Citterio and Piégay, 2009;

346 Gratzer *et al.*, 2020; Guntzel *et al.,* 2020; Guo *et al.*, 2023). Although it is clear that

347 groundwater contributions can mediate lake water surface areas, particularly during periods

348 of low flow (Song *et al.*, 2023; Bagheri *et al.*, 2024), these contributions cannot be resolved

349 from the satellite imagery, and so focus was directed to the controls of rainfall and channel-

350 floodplain complexes. Groundwater contributions are likely to be more important in lakes that

351 experience WSA growth deeper into the dry season, as shallow groundwater seeps into the

352 surface to sustain low flows (Miguez-Macho and Fan, 2012a, 2012b). However, surface water

353 hydrology in this region will be dominated by flood magnitude, particularly in setting the upper

354 limit on annual WSA extent (Miguez-Macho and Fan, 2012a; Bagheri *et al.*, 2024).

355 Total seasonal rainfall was limited in explaining WSA variations across the lakes, although a

356 weakly positive increase in WSA was observed with increasing rainfall (**Fig. 12b**). The main

357 challenge with this interpretation is the data variability, with varying rainfall magnitudes

358 invoking the same WSA response. Translating observed rainfall to WSA change is reliant upon

359 direct transmission into the lakes, which is possible when sourced overhead, but more

360 complicated when filtered through dense tree canopies (Zheng and Jia, 2020), where

361 interception can be as high as 25%, as reported in the Malaysian rainforest (Cleophas *et al.*,

362 2022). Equally complex is the routing of surface water through densely vegetated floodplain

363 and into the lakes. Floodplain roughness, vegetal uptake, and channelisation all present

364 challenges in connecting localised measurements of rainfall to changes in WSA, since these

365 processes can repartition water to different parts of the floodplain (Mertes, 1997; Tabacchi *et*

366 *al.*, 2000; Harvey *et al.*, 2009; David *et al.*, 2018).

367 Since rainfall patterns are unable to fully explain changes in WSA, flood-driven channel-

368 floodplain interactions must play a crucial role in mediating WSAs through time. During the

369 wet season water levels on the Beni and Mamoré rise by ~10 m, triggering overbank flows

370 that reactivate tie channels, which can transmit substantial quantities of sediment-laden water

371 into the floodplain (Day *et al.*, 2008). Gradients of hydrological exchange should be controlled

372 by proximity to the mainstem, with lakes close to the channel experiencing larger WSA

373 variations in response to the rising flood pulse. This pattern can be observed on the Beni and

374 Mamoré, although there is considerable noise for lakes situated within 1 km of the mainstem

15

375 (**Fig. 13a**). Some of this noise can be attributed to incursion – where the active channel

376 migrates into the year 1 WSA boundary; in these cases, proximity values were set to 0 m (n =

377 87 of 809 unique measurements), resulting in a range of WSAs for the same proximity.

378 Most lakes were situated within 1 km of the active channel and experienced the largest range

379 of WSAs (**Fig. 13b,c**). This behaviour was observed for both neck- and chute-derived lakes

380 indicating that flow advection from the channel was large enough to overcome morphological

381 differences between the lakes (e.g., divergence angle and sedimentary plug characteristics)

382 (Shields and Abt, 1989; Richards *et al.*, 2022) . Although, some of the fundamental differences

383 between lake type explain the range of WSA changes observed over interannual timescales

384 (**Fig. 10**). Chute lakes typically convey greater proportions of discharge post-cutoff due to

385 shallower divergence angles and slower plug formation, thus feasibly allowing for faster

386 sequences of filling and draining, relative to the rise and fall of the flood pulse, compared to

387 neck-derived lakes (Allen, 1965). This also explains why the relationship between total

388 seasonal rainfall and WSA was stronger for chute lakes than it was for necks (**Fig. 12b**) and

389 is likely indicative of changes in channel hydrology driven by rainfall fluctuations. As distance

390 from the mainstem increased, WSA variability (represented by the standard deviation; **Fig.**

391 **13c**), diminished, although several lakes still experienced comparable WSA variations to lakes

392 situated 27 times (~1.43 km) closer to the channel. Mechanistically, these changes must be

393 driven by water sourced from tie channels (Rowland *et al.*, 2009), the perirheic zone (Mertes,

394 1997), or groundwater (Bagheri *et al.*, 2024).

395 The majority of lakes in the dataset were associated with tie channels (551 instances from a

396 total of 809 measurements) and displayed the largest variations in WSA (1.3 times and 3.9

397 times larger than incursion and isolated lakes, respectively) (**Fig. 14**). The wide range of WSAs

398 for these type of lakes demonstrates the propensity of tie channels to effectively transmit water

399 away from the mainstem during floods (~30 – > 4000 m). This results in highly localised WSA

400 changes linked to the morphology of the tie channels (i.e., length, width, and depth), rather

401 than systematic trends with streamwise distance or lake type (**e.g., Fig. 9a,b**). Moreover, lake

402   age is observed to be independent of changes in WSA variation, since tie channels can form

403   and maintain hydrological connectivity on lakes of any age (**Fig. 9c**). Resultantly, the WSA of

404   lakes connected by tie channels could rapidly diminish in size as sediment-laden water begins

405   to the fill the basin (Rowland *et al.*, 2005). Alternatively, the rate of infill may be distorted as

406   interannual fluctuations – driven by seasonal floodwater incursion – is interpreted as a stable

407   or increasing WSA through time. The ability of tie channels to annually prograde into the lake

408   can extend the area of influence over which hydrological changes occur and shifts the focus

409   of where site specific changes in lake area occur. Rowland et al. (2005) reported channel

410   extension rates of between 1 and 133 m yr^{-1} for two rivers in the United States and one in

411   Papua New Guinea. A deeper elucidation of the differences in tie channel morphology and

412   how these impact lake WSAs is precluded by image resolution in the present study, since tie

413   channels were consistently at a scale equal or finer than 30 m/pixel.

414   Incursion was the second most common lake type (219 of 809), highlighting the significant

415   rate of floodplain recycling occurring along meandering rivers and the propensity for

416   abandoned channels to be reactivated by channel migration (Constantine *et al.*, 2014; Guo *et*

417   *al.*, 2023). Variations in WSA were similarly large for these type of lakes, although maximum

418   WSAs were generally lower, reflecting the inherent reduction in lake surface area through

419   erosion. Before incursion occurred, tie channels connected all of the lakes to the mainstem,

420   which may explain the similar range of WSAs for both populations of lakes as the lake area

421   remains approximately the same after incursion. Moreover, incursion improves hydrological

422   connectivity, by increasing the size of the entrance to the lake. When floodwaters recede, the

423   enlarged entrance serves as a drainage outlet, allowing return flows to drain the lake at a

424   feasibly greater rate than if return flows were limited to the discharge rate of tie channels alone.

425   Despite incursion reflecting the migration of the active channel through the lake boundary,

426   instances are observed up to 2.2 km away from the mainstem and occurs, on average, when

427   the channel is 447 m away from the lake boundary. These instances can be explained by

428   sensitivity of the measurements to classification criteria: first, long-distance incursions can

429   occur where the active channel breaches an oxbow lake and is subsequently cut off, leaving

430   the original lake incursion intact. Second, proximity of the mainstem to the year 1 WSA is

431   inherently underestimated by around 0.5 channel widths when using the channel centreline

432   (see **Methods** for more information).

433   Only 39 instances of isolated lakes were documented in the dataset and were found to be

434   further away from the active channel (up to 4.1 km). The small range of WSAs for these lakes

435   can be explained by the absence of observable flow pathways linking them to the active

436   channel. In these instances, the interaction between pluvial and fluvial floodwater may be a

437   more important control on WSA variations as the storage capacity of the floodplain diminishes

438   and lakes offer topographically favourable sites for convergence (Tull *et al.*, 2022). WSA

439   reductions are likely controlled by evaporative losses, peaking at the transition from dry to wet

440   season in September - November, since evidence for surficial drainage is absent (Martinelli *et*

441   *al.*, 1996; Fleischmann *et al.*, 2023). While suppressed peaks in WSA may be indicative of

442   reduced flood peaks on the channel (Guo *et al.*, 2023), groundwater infiltration is also likely to

443   be more important for WSA variations where channel connectivity and floodplain flows are

444   minimal (Gratzer *et al.*, 2020).

445   **Implications**

446   Diverse hydrological behaviour is crucial for the functioning of oxbow lakes and the provision

447   of ecosystem services that sustain riparian wildlife, vegetation, and communities (Obolewski

448   *et al.*, 2009; Thomaz *et al.*, 2009; Lizarro *et al.*, 2020). This diversity is set by the water balance

449   of individual lakes, which in turn, is set by the mechanisms controlling water entry and exit.

450   The direct transmission of exogenous water into oxbow lakes stimulates physiochemical

451   heterogeneity, triggered by diffusive mixing at the channel-lake interface (in the case of

452   incursion lakes), similar to the active meander or early cutoff stages outlined by Gagliano and

453   Howard (1983), or when a turbulent jet enters the lake through a tie channel (Day *et al.*, 2008).

454   River water will be well-mixed relative to the lakes – where stratification may have developed

455   after flood waters recede – with higher concentrations of dissolved oxygen, turbidity,

conductivity, organic carbon, and other essential nutrients (e.g., nitrogen and phosphorus) (Van den Brink *et al.,* 1992). The influx of these nutrient-rich waters stimulates primary productivity and sustenance for the wider riparian food web (Kufel and Leśniczuk, 2014; Miranda *et al.*, 2014); although, nutrient loading can present a challenge when lakes become eutrophic, and dissolved oxygen supplies diminish (Obolewski *et al.*, 2016). Reconciling source water physiochemistry with mechanisms of water transmission could help identify sites at risk from stratification and anoxia, where economic or subsistence fishing yields would be limited. Nutrient-rich sites should also be locations of maximum carbon burial, as respired organic matter and suspended mineral carbon is deposited on the lake bed. However, this process is reliant on the physiochemical characteristics of the water which, under certain conditions (e.g., hypoxia), may trigger negative biogeochemical transformations (e.g., methane production), thus offsetting any stores of sequestered carbon (Pierobon *et al.*, 2010; Debanshi and Pal, 2022).

In addition to carbon trapping, oxbow lakes can sequester industrial and agricultural contaminants (e.g., mercury from artisanal gold mining, polychlorinated biphenyls, and excess nitrate and phosphate leached from farmland) (Schilling *et al.*, 2019; Thomas *et al.*, 2021; Nifong *et al.*, 2022; Barocas *et al.*, 2023). The lakes effectively filter the fine-grained suspended sediments on which these contaminants bind from the river system, but continue to pose a threat to lacustrine wildlife through direct absorption and biomagnification (Bastos *et al.*, 2015; Barocas *et al.*, 2023) or biochemical transformation in concert with changing physiochemical properties (e.g., anoxia) (Eckley and Hintelmann, 2006). Lakes with large WSA variations should be prioritised as sites most at risk of promoting food web contamination, particularly where suspended sediment deposition is precluded by lake physiochemistry and is susceptible to re-released back into the river channel (Wren *et al.*, 2019). Results from the present study suggest that chute-lakes are most at-risk sites for nutrient and contaminant remobilisation since they maintain greater hydrological connectivity and WSA variations. Future land use changes could amplify this risk along river corridors as

483   changes in floodplain roughness (indicative of changes from forest to pasture) have

484   associated with an increase in chute channel formation (Lazarus and Constantine, 2013;

485   Lewis *et al.*, 2020).

486   Differences in lake connectivity will also be archived in the stratigraphic record of lake-bed

487   sediments. Typically, grain-size fining is observed with distance from the lake entrance, as

488   sediment conveyance diminishes with decreasing flow velocity (Fisk, 1947); however, where

489   flow conveyance is maintained (e.g., from tie channels or after incursion), existing deposits

490   can be eroded and redistributed, thus changing the expected pattern of deposition in the bed

491   sediments (Toonen *et al.*, 2012). Reconciling these processes with knowledge of where

492   nutrient loading is highest in the bed will improve forecasting sites of contaminant

493   remobilisation and habitat degradation. Moreover, these sites should be recommended to

494   community stakeholders as at risk sites for wildlife and humans. Isolated lakes within the same

495   river corridor should act as baseline sites from which comparisons of sedimentology,

496   physiochemistry and biodiversity can be made, since the processes controlling WSA

497   variations will be less dependent on channel hydrology. Notwithstanding, organic and

498   inorganic contributions transferred from the floodplain into isolated lakes must still be

499   considered as a contaminant source that may impact lake ecology (Ahearn *et al.*, 2006).

500   Finally, a process understanding of the controls on oxbow lake hydrodynamics is crucial for

501   forecasting how climatic or human-induced changes in catchment hydrology may disrupt the

502   natural functioning of these habitats (Latrubesse *et al.*, 2020). Flow regulation will reduce the

503   magnitude of the flood pulse, thus limiting hydrological exchange between the channel and

504   floodplain wetlands. Moreover, a reduction in hydrological connectivity will decrease the

505   nutrient and sediment supply to lakes, limiting their ability to filter contaminants and sequester

506   organic and inorganic material, and reduce migratory pathways for wildlife. Likewise, changes

507   in regional climate could intensify droughts and floods, altering lake physiochemistry, and

508   potentially converting lakes from biodiversity hotspots to dead zones. These impacts would

509   be compounded by the effects of flow regulation and land-use conversion.

Conclusions

Oxbow lakes serve as critical ecotones for aquatic and terrestrial wildlife and provide a range of important ecosystem services that function to purify river systems and sequester organic and inorganic particulates, while enhancing biodiversity. The provision of these services are driven by interactions between the river and lakes after cutoff. Over annual and interannual timescales, lakes display considerable hydrological variability, manifested through changes in water surface area (WSA). The proximity of lakes to the river channel was found to be a key control on WSA changes, although the mechanism for water transmission into the lakes was key to explaining variability in the data. Most lakes maintain hydrological connectivity through tie channels, which can extend deep into the floodplain, while others remain relatively undisturbed by the river channel, and which are likely hydrologically controlled by precipitation, groundwater, or the routing of water across the floodplain. Lakes that experienced incursion – where the active channel migrates into the lake – could convey more water and behaved similar to those connected by tie channels. Chute channels showed a wider range of WSAs and impacted by mainstem connectivity much further away than neck-lakes. Understanding the controls on WSA changes in oxbow lakes is essential for quantifying biogeochemical fluxes in wetland systems and for prioritising sites most at risk of nutrient and contaminant release, which may cause water quality deterioration and risk to human health. Importantly, an understanding of the process controls on lake hydrodynamics is essential for forecasting the impacts changes in catchment hydrology on floodplain wetlands.

Data availability

Data is available on request to the author.

References

Aalto R, Maurice-Bourgoin L, Dunne T, Montgomery DR, Nittrouer CA, Guyot J-L. 2003.
    Episodic sediment accumulation on Amazonian flood plains influenced by El
    Nino/Southern Oscillation. *Nature* **425**: 493–497

Ahearn DS, Viers JH, Mount JH, Dahlgreen RA. 2006. Priming the productivity pump: flood
    pulse driven trends in suspended algal biomass distribution across a restored
    floodplain. *Freshwater Biology* **51** (8): 1417–1433 DOI: 10.1111/j.1365-
    2427.2006.01580.x

Ahmed J, Constantine JA, Dunne T. 2019. The role of sediment supply in the adjustment of
    channel sinuosity across the Amazon Basin. *Geology* **47** (9): 807–810 DOI:
    10.1130/G46319.1

Allen JRL. 1965. A review of the origin and characteristics of recent alluvial sediments.
    Sedimentology **5**: 89–191

Anderson EP, Jenkins CN, Heilpern S, Maldonado-Ocampo JA, Carvajal-Vallejos FM,
    Encalada AC, Rivadeneira JF, Hidalgo M, Cañas CM, Ortega H, et al. 2018.
    Fragmentation of Andes-to-Amazon connectivity by hydropower dams. *Science
    Advances* **4** (1): eaao1642–eaao1642 DOI: 10.1126/sciadv.aao1642

Arantes CC, Laufer J, Pinto MD da S, Moran EF, Lopez MC, Dutka-Gianelli J, Pinto DM,
    Chaudhari S, Pokhrel Y, Doria CRC. 2022. Functional responses of fisheries to
    hydropower dams in the Amazonian Floodplain of the Madeira River. *Journal of
    Applied Ecology* **59** (3): 680–692 DOI: 10.1111/1365-2664.14082

Bagheri O, Pokhrel Y, Moore N, Phanikumar MS. 2024. Groundwater dominates terrestrial
    hydrological processes in the Amazon at the basin and subbasin scales. *Journal of
    Hydrology* **628**: 130312 DOI: 10.1016/j.jhydrol.2023.130312

Barocas A, Vega C, Alarcon Pardo A, Araujo Flores JM, Fernandez L, Groenendijk J,
    Pisconte J, Macdonald DW, Swaisgood RR. 2023. Local intensity of artisanal gold

561   mining drives mercury accumulation in neotropical oxbow lake fishes. *Science of The*

562   *Total Environment* **886**: 164024 DOI: 10.1016/j.scitotenv.2023.164024

563 Bastos WR, Dórea JG, Bernardi JVE, Lauthartte LC, Mussy MH, Hauser M, Dória CR da C,

564   Malm O. 2015. Mercury in muscle and brain of catfish from the Madeira river,

565   Amazon, Brazil. *Ecotoxicology and Environmental Safety* **118**: 90–97 DOI:

566   10.1016/j.ecoenv.2015.04.015

567 Bookhagen B, Strecker MR. 2008. Orographic barriers, high-resolution TRMM rainfall, and

568   relief variations along the eastern Andes. *Geophysical Research Letters* **35** (6) DOI:

569   10.1029/2007GL032011

570 Bookhagen B, Strecker MR. 2010. Modern Andean Rainfall Variation during ENSO Cycles

571   and its Impact on the Amazon Drainage Basin. In *Amazonia: Landscape and Species*

572   *Evolution*Wiley-Blackwell Publishing Ltd.; 223–241. DOI:

573   10.1002/9781444306408.ch14

574 Bourrel L, Phillips L, Moreau S. 2009. The dynamics of floods in the Bolivian Amazon Basin.

575   *Hydrological Processes* **23**: 3161–3167 DOI: 10.1002/hyp.7384

576 Bridge JS, Smith ND, Trent F, Gabel SL, Bernstein P. 1986. Sedimentology and morphology

577   of a low-sinuosity river: Calamus River, Nebraska Sand Hills. *Sedimentology* **33**:

578   851–870 DOI: 10.1111/j.1365-3091.1986.tb00987.x

579 Citterio A, Piégay H. 2009. Overbank sedimentation rates in former channel lakes:

580   characterization and control factors. *Sedimentology* **56** (2): 461–482 DOI:

581   10.1111/j.1365-3091.2008.00979.x

582 Cleophas F, Mahali M, Musta B, Zahari NZ, Lee LE, Bidin K. 2022. Canopy precipitation

583   interception in a lowland tropical forest in relation to stand structure. *IOP Conference*

584   *Series: Earth and Environmental Science* **1053** (1): 012005 DOI: 10.1088/1755-

585   1315/1053/1/012005

586 Constantine JA, Dunne T. 2008. Meander cutoff and the controls on the production of oxbow

587   lakes. *Geology* **36**: 23–26

588 Constantine JA, Dunne T, Ahmed J, Legleiter C, Lazarus ED. 2014. Sediment supply as a

589   driver of river meandering and floodplain evolution in the Amazon Basin. *Nature*

590   *Geoscience* **7** (12): 899–903 DOI: 10.1038/ngeo2282

591 Constantine JA, Dunne T, Piégay H, Mathias Kondolf G. 2010a. Controls on the alluviation

592   of oxbow lakes by bed-material load along the Sacramento River, California.

593   *Sedimentology* **57**: 389–407 DOI: 10.1111/j.1365-3091.2009.01084.x

594 Constantine JA, McLean SR, Dunne T. 2010b. A mechanism of chute cutoff along large

595   meandering rivers with uniform floodplain topography. *Geological Society of America*

596   *Bulletin* **122**: 855–869 DOI: 10.1130/b26560.1

597 David SR, Czuba JA, Edmonds DA. 2018. Channelization of meandering river floodplains by

598   headcutting. *Geology* **47** (1): 15–18 DOI: 10.1130/G45529.1

599 Day G, Dietrich WE, Rowland JC, Marshall A. 2008. The depositional web on the floodplain

600   of the Fly River, Papua New Guinea. *Journal of Geophysical Research: Earth*

601   *Surface* **113** (F1) DOI: 10.1029/2006JF000622

602 Debanshi S, Pal S. 2022. Assessing the role of deltaic flood plain wetlands on regulating

603   methane and carbon balance. *Science of The Total Environment* **808**: 152133 DOI:

604   10.1016/j.scitotenv.2021.152133

605 Dieras PL. 2013. The persistence of oxbow lakes as aquaic habitatas: an assessment of

606   ratesof change and patterns of alluviation Available at: http://orca.cf.ac.uk/49392/

607 Dieras PL, Constantine JA, Hales TC, Piégay H, Riquier J. 2013. The role of oxbow lakes in

608   the off-channel storage of bed material along the Ain River, France. *Geomorphology*

609   DOI: 10.1016/j.geomorph.2012.12.024

610 Eckley CS, Hintelmann H. 2006. Determination of mercury methylation potentials in the

611   water column of lakes across Canada. *Selected papers from the 7th International*

612   *Conference on Mercury as a Global Pollutant, Ljubljana, Slovenia June 27 - July 2,*

613   *2004* **368** (1): 111–125 DOI: 10.1016/j.scitotenv.2005.09.042

614 Espinoza JC, Marengo JA, Ronchail J, Carpio JM, Flores LN, Guyot JL. 2014. The extreme

615   2014 flood in south-western Amazon basin: the role of tropical-subtropical South

616   Atlantic SST gradient. *Environmental Research Letters* **9**: 124007–124007

617 Espinoza JC, Ronchail J, Frappart F, Lavado W, Santini W, Guyot JL. 2013. The Major

618   Floods in the Amazonas River and Tributaries (Western Amazon Basin) during the

619   1970–2012 Period: A Focus on the 2012 Flood*. *Journal of Hydrometeorology* **14**:

620   1000–1008 DOI: 10.1175/JHM-D-12-0100.1

621 Finer M, Jenkins CN. 2012. Proliferation of hydroelectric dams in the Andean Amazon and

622   implications for Andes-Amazon connectivity. *PLOS One* **7**: e35126–e35126 DOI:

623   10.1371/journal.pone.0035126

624 Fisk HN. 1947. Fine-grained alluvial deposits and their effects upon mississippi river activity.

625   *Waterways Experiment Station*: 82–82

626 Fleischmann AS, Laipelt L, Papa F, Paiva RCD de, de Andrade BC, Collischonn W, Biudes

627   MS, Kayser R, Prigent C, Cosio E, et al. 2023. Patterns and drivers of

628   evapotranspiration in South American wetlands. *Nature Communications* **14** (1):

629   6656 DOI: 10.1038/s41467-023-42467-0

630 Fleischmann AS, Papa F, Fassoni-Andrade A, Melack JM, Wongchuig S, Paiva RCD,

631   Hamilton SK, Fluet-Chouinard E, Barbedo R, Aires F, et al. 2022. How much

632   inundation occurs in the Amazon River basin? *Remote Sensing of Environment* **278**:

633   113099 DOI: 10.1016/j.rse.2022.113099

634 Gagliano SM, Howard PC. 1984. The neck cutoff oxbow lake cycle along the Lower

635   Mississippi River. In *River Meandering*ASCE; 147–158.

636 Gautier E, Brunstein D, Vauchel P, Roulet M, Fuertes O, Guyot JL, Darozzes J, Bourrel L.

637   2007. Temporal relations between meander deformation, water discharge and

638   sediment fluxes in the floodplain of the Rio Beni (Bolivian Amazonia). *Earth Surface*

639   *Processes and Landforms* **32**: 230–248 DOI: 10.1002/esp.1394

640 Gay GR, Gay HH, Gay WH, Martinson HA, Meade RH, Moody JA. 1998. Evolution of cutoffs

641   across meander necks in Powder River, Montana, USA. *Earth Surface Processes*

and Landforms **23**: 651–662 DOI: 10.1002/(sici)1096-9837(199807)23:7<651::aid-esp891>3.0.co;2-v

Gorelick N, Hancher M, Dixon M, Ilyushchenko S, Thau D, Moore R. 2017. Google Earth Engine: Planetary-scale geospatial analysis for everyone. *Big Remotely Sensed Data: tools, applications and experiences* **202**: 18–27 DOI: 10.1016/j.rse.2017.06.031

Gratzer MC, Davidson GR, O'Reilly AM, Rigby JR. 2020. Groundwater recharge from an oxbow lake-wetland system in the Mississippi Alluvial Plain. *Hydrological Processes* **34** (6): 1359–1370 DOI: 10.1002/hyp.13680

Grenfell M, Aalto R, Nicholas A. 2012. Chute channel dynamics in large, sand-bed meandering rivers. *Earth Surface Processes and Landforms* **37**: 315–331

Guntzel AM, Marcos da Silva W, Panarelli EA. 2020. Connectivity as the control key to intensity of flood pulse in Taquari River oxbow lakes. *Ambiente & Água - An Interdisciplinary Journal of Applied Science* **15** (4): 12

Guo X, Gao P, Li Z. 2023. Hydrologic connectivity and morphologic variation of oxbow lakes in a pristine alpine fluvial system. *Journal of Hydrology* **623**: 129768 DOI: 10.1016/j.jhydrol.2023.129768

Guyot JL, Fillzola N, Quintanilla J, Cortez J. 1996. Dissolved solids and suspended sediment yields in the Rio Madeira basin, from the Bolivian Andes to the Amazon. *IAHS Publication*: 55–64

Hamilton SK, Sippel SJ, Melack JM. 2004. Seasonal inundation patterns in two large savanna floodplains of South America: the Llanos de Moxos (Bolivia) and the Llanos del Orinoco (Venezuela and Colombia). *Hydrological Processes* **18** (11): 2103–2116 DOI: 10.1002/hyp.5559

Harvey JW, Schaffranek RW, Noe GB, Larsen LG, Nowacki DJ, O'Connor BL. 2009. Hydroecological factors governing surface water flow on a low-gradient floodplain. *Water Resources Research* **45** (3) DOI: 10.1029/2008WR007129

668 Hooke JM. 1995. River channel adjustment to meander cutoffs on the River Bollin and River
669   Dane, northwest England. *Geomorphology* **14**: 235–253 DOI: 10.1016/0169-
670   555x(95)00110-q

671 Jaeger KL, Olden JD, Pelland NA. 2014. Climate change poised to threaten hydrologic
672   connectivity and endemic fishes in dryland streams. *Proceedings of the National*
673   *Academy of Sciences* **111** (38): 13894–13899 DOI: 10.1073/pnas.1320890111

674 Killeen TJ, Douglas M, Consiglio T, Jørgensen PM, Mejia J. 2007. Dry spots and wet spots
675   in the Andean hotspot. *Journal of Biogeography* **34** (8): 1357–1373 DOI:
676   10.1111/j.1365-2699.2006.01682.x

677 Kufel L, Leśniczuk S. 2014. Hydrological connectivity as most probable key driver of
678   chlorophyll and nutrients in oxbow lakes of the Bug River (Poland). *Limnologica* **46**:
679   94–98 DOI: 10.1016/j.limno.2013.10.008

680 Latrubesse EM, Arima EY, Dunne T, Park E, Baker VR, d'Horta FM, Wight C, Wittmann F,
681   Zuanon J, Baker PA, et al. 2017. Damming the rivers of the Amazon basin. *Nature*
682   **546** (7658): 363–369 DOI: 10.1038/nature22333

683 Latrubesse EM, D'Horta FM, Ribas CC, Wittmann F, Zuanon J, Park E, Dunne T, Arima EY,
684   Baker PA. 2020. Vulnerability of the biota in riverine and seasonally flooded habitats
685   to damming of Amazonian rivers. *Aquatic Conservation: Marine and Freshwater*
686   *Ecosystems* DOI: 10.1002/aqc.3424

687 Lauer JW, Parker G. 2008. Net local removal of floodplain sediment by river meander
688   migration. *Geomorphology* **96**: 123–149

689 Lazarus E, Constantine JA. 2013. Generic theory for channel sinuosity. *Proceedings of the*
690   *National Academy of Sciences* **110** (21): 8447–8452

691 Lewin J, Ashworth PJ. 2014. The negative relief of large river floodplains. *Earth-Science*
692   *Reviews* **129**: 1–23 DOI: 10.1016/j.earscirev.2013.10.014

693 Lewis GW, Lewin JOP-IA of SSP. 1983. Alluvial cutoffs in Wales and the Borderlands (JD
694   Collinson and J Lewin, eds). *Modern and ancient fluvial systems* **6**: 145–154

695 Lewis QW, Edmonds DA, Yanites BJ. 2020. Integrated UAS and LiDAR reveals the

696   importance of land cover and flood magnitude on the formation of incipient chute

697   holes and chute cutoff development. *Earth Surface Processes and Landforms* **45** (6):

698   1441–1455 DOI: 10.1002/esp.4816

699 Lizarro D, Pinto-Viveros MA, Moreno-Aulo F. 2020. Comunidad de peces de la laguna de

700   inundación urbana Las Palquitas, Trinidad-Beni (Bolivia). *Ecología en Bolivia* **55**:

701   210–225

702 Marengo JA, Espinoza JC. 2016. Extreme seasonal droughts and floods in Amazonia:

703   causes, trends and impacts. *International Journal of Climatology* **36** (3): 1033–1050

704   DOI: 10.1002/joc.4420

705 Martinelli LA, Victoria RL, Silveira Lobo Sternberg L, Ribeiro A, Zacharias Moreira M. 1996.

706   Using stable isotopes to determine sources of evaporated water to the atmosphere in

707   the Amazon basin. *Journal of Hydrology* **183** (3): 191–204 DOI: 10.1016/0022-

708   1694(95)02974-5

709 Mertes LAK. 1997. Documentation and significance of the perirheic zone on inundated

710   floodplains. *Water Resources Research* **33**: 1749–1762 DOI: 10.1029/97WR00658

711 Miguez-Macho G, Fan Y. 2012a. The role of groundwater in the Amazon water cycle: 1.

712   Influence on seasonal streamflow, flooding and wetlands. *Journal of Geophysical*

713   *Research: Atmospheres* **117** (D15) DOI: 10.1029/2012JD017539

714 Miguez-Macho G, Fan Y. 2012b. The role of groundwater in the Amazon water cycle: 2.

715   Influence on seasonal soil moisture and evapotranspiration. *Journal of Geophysical*

716   *Research: Atmospheres* **117** (D15) DOI: 10.1029/2012JD017540

717 Miranda LE, Andrews CS, Kröger R. 2014. Connectedness of land use, nutrients, primary

718   production, and fish assemblages in oxbow lakes. *Aquatic Sciences* **76** (1): 41–50

719   DOI: 10.1007/s00027-013-0310-y

720 Nielsen DL, Merrin LE, Pollino CA, Karim F, Stratford D, O'Sullivan J. 2020. Climate change

721   and dam development: Effects on wetland connectivity and ecological habitat in

722   tropical wetlands. *Ecohydrology* **13** (6): e2228 DOI: 10.1002/eco.2228

723   Nifong RL, Taylor JM, DeVilbiss S. 2022. Spatial and temporal patterns of benthic nutrient

724   cycling define the extensive role of internal loading in an agriculturally influenced

725   oxbow lake. *Biogeochemistry* **159** (3): 413–433 DOI: 10.1007/s10533-022-00935-7

726   NOAA. 2024. Southern Oscillation Index Available at:

727   https://www.ncei.noaa.gov/access/monitoring/enso/soi [Accessed 18 July 2024]

728   Obolewski K, Glinska-Lewczuk K, Burandt P, Kobus S, Strzelczak A, Timofte C. 2016.

729   Response of the fish community to oxbow lake restoration in a low-gradient river

730   floodplain. *Environmental Engineering and Management Journal; Vol 15, No 6 (2016)*

731   Available at: https://www.eemj.eu/index.php/EEMJ/article/view/2948

732   Obolewski K, Glińska-Lewczuk K, Kobus S. 2009. Effect of hydrological connectivity on the

733   molluscan community structure in oxbow lakes of the Łyna River. *Oceanological and*

734   *Hydrobiological Studies* **38** (4): 75–88 DOI: 10.2478/v10009-009-0045-1

735   Ovando A, Martinez JM, Tomasella J, Rodriguez DA, von Randow C. 2018. Multi-temporal

736   flood mapping and satellite altimetry used to evaluate the flood dynamics of the

737   Bolivian Amazon wetlands. *International Journal of Applied Earth Observation and*

738   *Geoinformation* **69**: 27–40 DOI: 10.1016/j.jag.2018.02.013

739   Ovando A, Tomasella J, Rodriguez DA, Martinez JM, Siqueira-Junior JL, Pinto GLN, Passy

740   P, Vauchel P, Noriega L, von Randow C. 2016. Extreme flood events in the Bolivian

741   Amazon wetlands. *Journal of Hydrology: Regional Studies* **5**: 293–308 DOI:

742   10.1016/j.ejrh.2015.11.004

743   Pierobon E, Bolpagni R, Bartoli M, Viaroli P. 2010. Net primary production and seasonal

744   CO2 and CH4 fluxes in a Trapa natans L. meadow. *Journal of Limnology* **69** (2):

745   225–234 DOI: 10.4081/jlimnol.2010.225

746   Richards D, Konsoer K. 2020. Morphologic adjustments of actively evolving highly curved

747   neck cutoffs. *Earth Surface Processes and Landforms* **45** (4): 1067–1081 DOI:

748   10.1002/esp.4763

749   Richards D, Konsoer K, Langendoen E, Ursic M, Constantine J. 2022. Depositional patterns

750   of slowly plugging neck cutoffs from core analysis and estimates of bedload

transport, White River, Arkansas. *Sedimentology* **69** (2): 568–591 DOI: 10.1111/sed.12915

Rowland JC, Dietrich WE, Day G, Parker G. 2009. Formation and maintenance of single-thread tie channels entering floodplain lakes: Observations from three diverse river systems. *Journal of Geophysical Research: Earth Surface* **114**: n/a-n/a DOI: 10.1029/2008JF001073

Rowland JC, Lepper K, Dietrich WE, Wilson CJ, Sheldon R. 2005. Tie channel sedimentation rates, oxbow formation age and channel migration rate from optically stimulated luminescence (OSL) analysis of floodplain deposits. *Earth Surface Processes and Landforms* **30** (9): 1161–1179 DOI: 10.1002/esp.1268

Saha S, Chukwuka AV, Mukherjee D, Saha NC, Adeogun AO. 2022. Hydrological connectivity, surface water quality and distribution of fish species within sub-locations of an urban oxbow lake, East India. *Watershed Ecology and the Environment* **4**: 44–58 DOI: 10.1016/j.wsee.2022.04.001

Scarabotti PA, Demonte LD, Pouilly M. 2017. Climatic seasonality, hydrological variability, and geomorphology shape fish assemblage structure in a subtropical floodplain. *Freshwater Science* **36** (3): 653–668 DOI: 10.1086/693441

Schilling KE, Wilke K, Pierce CL, Kult K, Kenny A. 2019. Multipurpose Oxbows as a Nitrate Export Reduction Practice in the Agricultural Midwest. *Agricultural & Environmental Letters* **4** (1): 190035 DOI: 10.2134/ael2019.09.0035

Schwendel AC, Cooper AH. 2021. Meander chute cutoff at an alluvial river facilitated by gypsum sinkholes. *Geomorphology* **393**: 107944–107944 DOI: 10.1016/j.geomorph.2021.107944

Shields FD, Abt SR. 1989. Sediment deposition in cutoff meander bends and implications for effective management. *Regulated Rivers: Research & Management* **4**: 381–396 DOI: 10.1002/rrr.3450040406

777 Sioli H. 1975. Amazon tributaries and drainage basins. In *Ecological Studies-Analysis and*

778 *Synthesis*, Jacobs J, , Lange OL, , Olson JS, , Wieser W (eds).Springer-Verlag: New

779 York; 199–213.

780 Song Y, Zhang Q, Melack JM, Li Y. 2023. Groundwater dynamics of a lake-floodplain

781 system: Role of groundwater flux in lake water storage subject to seasonal

782 inundation. *Science of The Total Environment* **857**: 159414 DOI:

783 10.1016/j.scitotenv.2022.159414

784 Sylvester Z, Durkin PR, Hubbard SM, Mohrig D. 2021. Autogenic translation and counter

785 point bar deposition in meandering rivers. *GSA Bulletin* DOI: 10.1130/B35829.1

786 Tabacchi E, Lambs L, Guilloy H, Planty-Tabacchi A-M, Muller E, Décamps H. 2000. Impacts

787 of riparian vegetation on hydrological processes. *Hydrological Processes* **14** (16–17):

788 2959–2976 DOI: 10.1002/1099-1085(200011/12)14:16/17<2959::AID-

789 HYP129>3.0.CO;2-B

790 Thomas S-S, Constantine JA, Dethier D, Thoman JW Jr, Racela J, Blau E, Landis JD. 2021.

791 The importance of oxbow lakes in the floodplain storage of pollutants. *Geology* **50**

792 (4): 392–396 DOI: 10.1130/G49427.1

793 Thomaz SM, Carvalho P, Padial AA, Kobayashi JT. 2009. Temporal and spatial patterns of

794 aquatic macrophyte diversity in the Upper Paraná River floodplain. *Brazilian Journal*

795 *of Biology* **69** (2): 617–625

796 Toonen WHJ, Kleinhans MG, Cohen KM. 2012. Sedimentary architecture of abandoned

797 channel fills. *Earth Surface Processes and Landforms* **37**: 459–472 DOI:

798 10.1002/esp.3189

799 Tull N, Passalacqua P, Hassenruck-Gudipati HJ, Rahman S, Wright K, Hariharan J, Mohrig

800 D. 2022. Bidirectional River-Floodplain Connectivity During Combined Pluvial-Fluvial

801 Events. *Water Resources Research* **58** (3): e2021WR030492 DOI:

802 10.1029/2021WR030492

803 Turnipseed C, Konsoer K, Richards D, Willson C. 2021. Numerical Modeling of Two-

804 Dimensional Hydrodynamics in a Highly Curving and Actively Evolving Neck Cutoff

805   Under Different Hydrologic Conditions. *Water Resources Research* **57** (2):

806   e2020WR027329-e2020WR027329 DOI: 10.1029/2020WR027329

807 Van den Brink FWB, De Leeuw JPHM, Van Der Velde G, Verheggen GM. 1992. Impact of

808   hydrology on the chemistry and phytoplankton development in floodplain lakes along

809   the Lower Rhine and Meuse. *Biogeochemistry* **19** (2): 103–128 DOI:

810   10.1007/BF00000798

811 Wren DG, Taylor JM, Rigby JR, Locke MA, Yasarer LMW. 2019. Short term sediment

812   accumulation rates reveal seasonal time lags between sediment delivery and

813   deposition in an oxbow lake. *Agriculture, Ecosystems & Environment* **281**: 92–99

814   DOI: 10.1016/j.agee.2019.05.007

815 Xu H. 2006. Modification of normalised difference water index (NDWI) to enhance open

816   water features in remotely sensed imagery. *International Journal of Remote Sensing*

817   **27** (14): 3025–3033 DOI: 10.1080/01431160600589179

818 Zheng C, Jia L. 2020. Global canopy rainfall interception loss derived from satellite earth

819   observations. *Ecohydrology* **13** (2): e2186 DOI: 10.1002/eco.2186

820 Zinger JA, Rhoads BL, Best JL. 2011. Extreme sediment pulses generated by bend cutoffs

821   along a large meandering river. **4**: 678

822
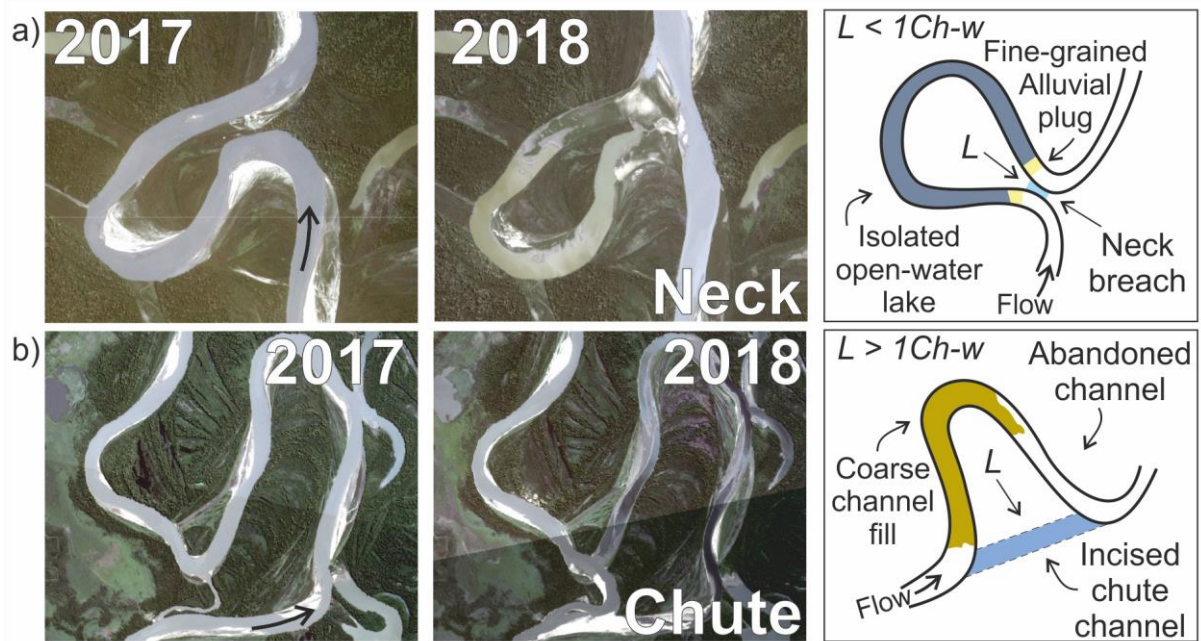
Figure 1. Mechanisms of cutoff formation. a) Neck cutoff on the Beni River between 2017 and 2018. The images show the termination of a meander bend by the convergence of two bends through a floodplain strip over a distance less than one channel width (*L < 1Ch-w*). b) Chute cutoff on the Mamoré River between 2017 and 2018. A chute channel captures a greater proportion of channel flow and enlarges causing abandonment of the former channel. Schematic representations of each cutoff mechanism are displayed in the far right panels. Flow directions are indicated by black arrows. Satellite images were acquired by PlanetLabs.
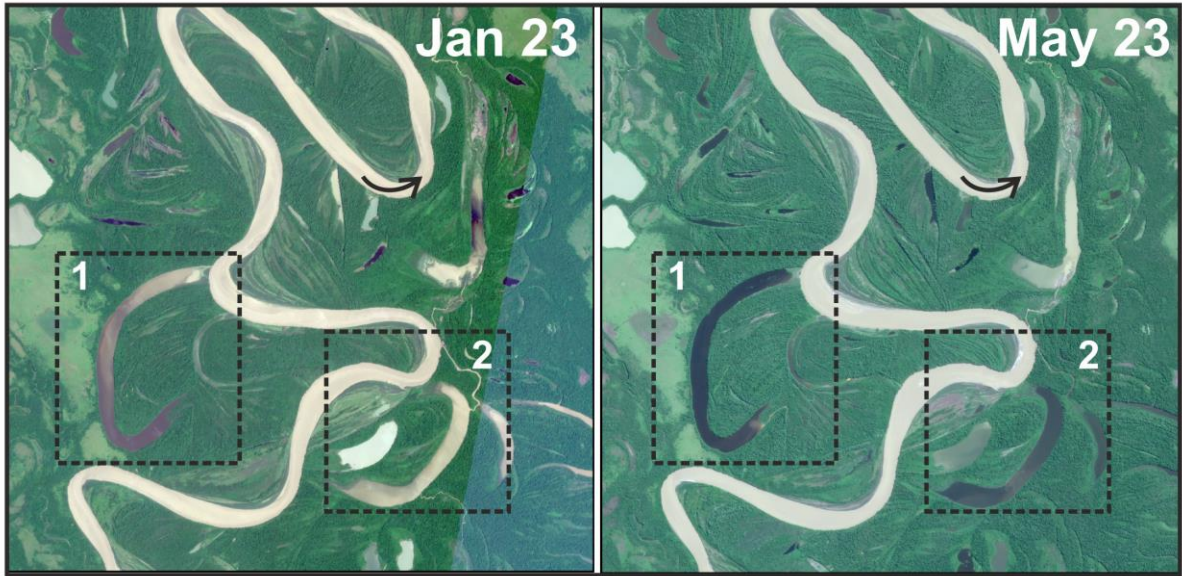
Figure 2. Examples of lake connectivity during floods. a) Two lakes (1) and (2) on the Mamoré River in January 2023. Turbid river water is observed mixing with the less turbid lake water through tie and floodplain channels. b) The same two lakes in May 2023 after flood waters have receded and connectivity to the mainstem had ceased. Black arrows indicate flow direction.
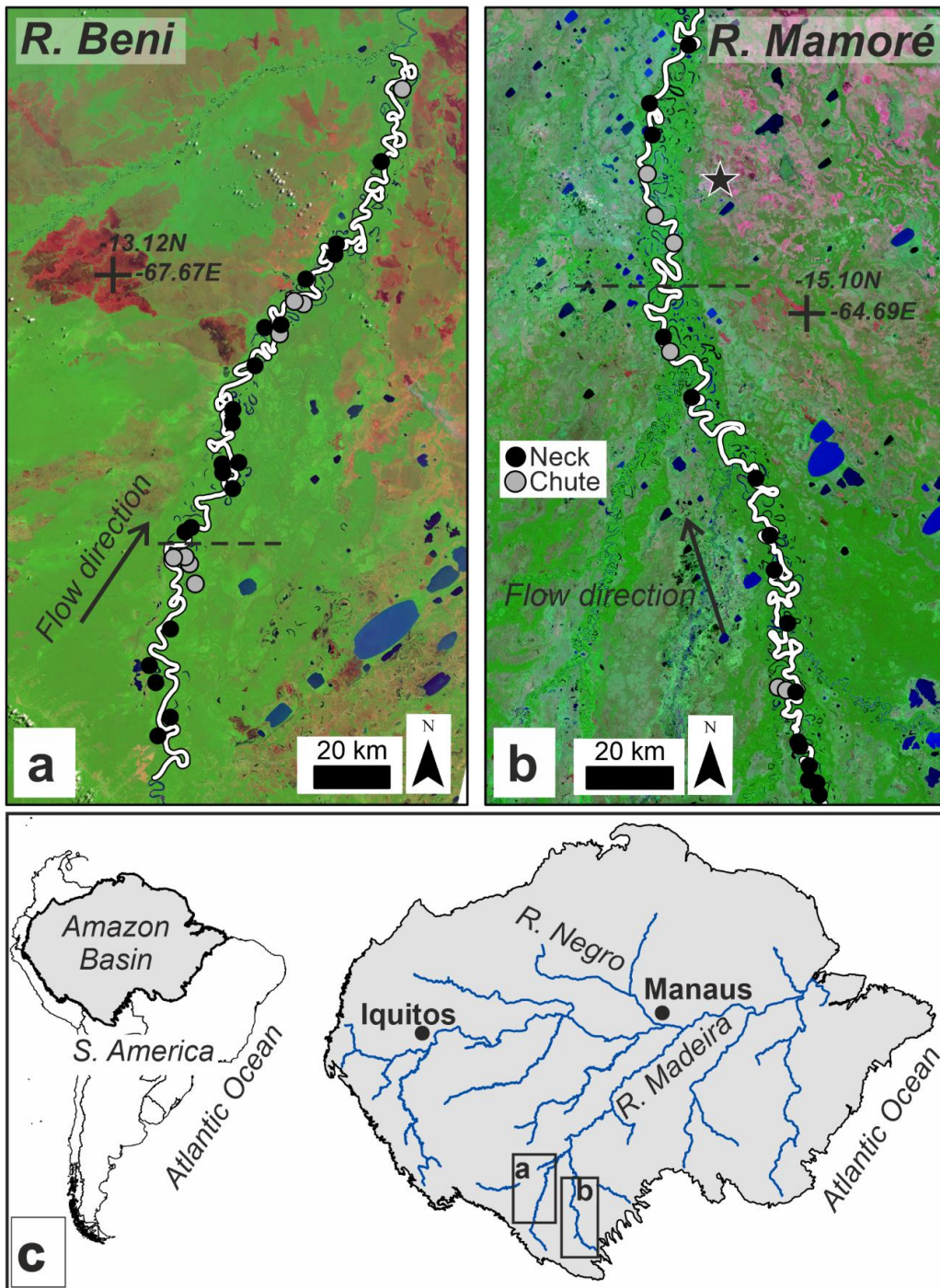
Figure 3. Studied oxbow lakes along the Rios Beni (a) and Mamoré (b) in Bolivia symbolised by cutoff type and formed between 1984 and 2022. Black points represent lakes formed through neck cutoff, while grey points represent those formed by chute cutoff. Flow direction is from south to north. The study sites' location within the Amazon Basin and South America (c). Black dashed lines indicate where the reach was split during the image acquisition stage.
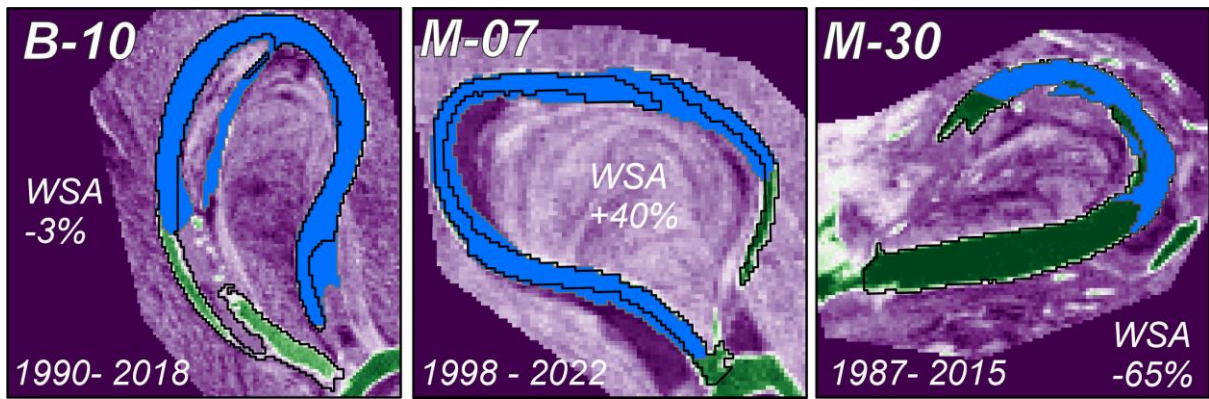
Figure 4. Computing water surface areas (WSAs) using the modified Normalised Difference Water Index (mNDWI). The mNDWI was computed for each year on record from cutoff inception (black outline) to demise or until the final year on record (blue shaded area; 2022). False-colour mNDWI images from the final year in each panel are used in the background where shades of purple indicate non-wetted areas and shades of green are wetted areas. Differences in lake area were computed at both annual and full-record resolution by measuring the relative change in area over the desired inspection period and normalising the lake area by centreline length in the year of formation.
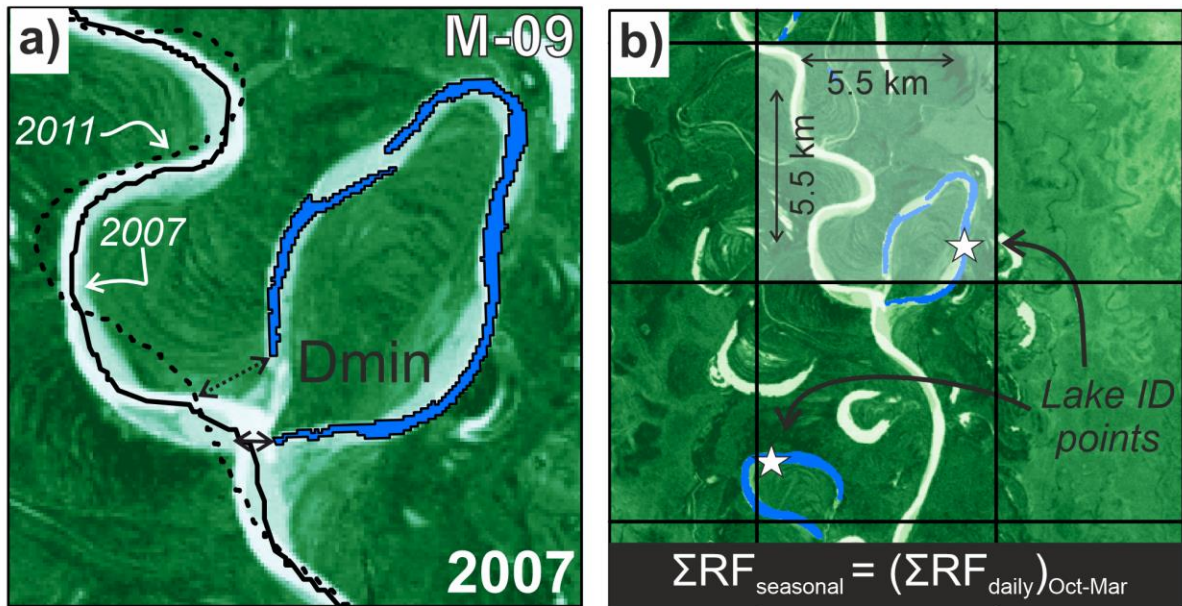
Figure 5. Methods for computing mainstem proximity and rainfall metrics. a) proximity was measured as the closest orthogonal distance from the mainstem centreline (black lines) and the boundary of the lake WSA (blue shaded area) in any given year. Pixel resolution is 30 m^2. b) Rainfall was computed at annual and seasonal resolution, where a single year was measured from October to September in accordance with the hydrological year. Rainfall data were extracted from 5.5 km^2 gridded total daily rainfall situated over each of the study lakes as collected by the Climate Hazards Group InfraRed Precipitation with Station data (CHIRPS) program. The total seasonal rainfall ($\Sigma RF_{seasonal}$) was computed as the sum of daily rainfall totals between October and March (($\Sigma RF_{daily})_{Oct-Mar}$), which corresponds to the wet season in Bolivia.
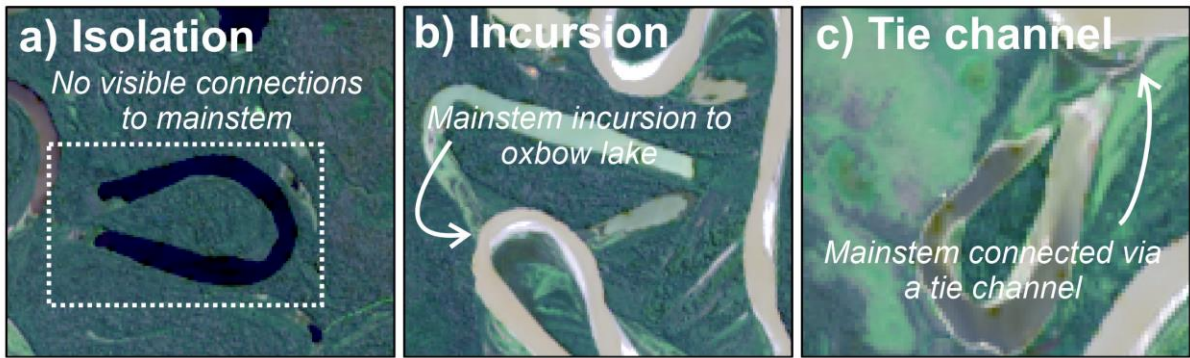
Figure 6. Lake connection styles. a) Isolation, where there are no clear visible connections between the lake and the active river channel; b) incursion, where the active channel breaches the year 1 lake boundary; and c) tie channel, where clear evidence of tie channels connecting the active channel to oxbow lakes is visible. Background images were obtained from Landsat Earth Explorer of the Rio Mamoré in 2023.
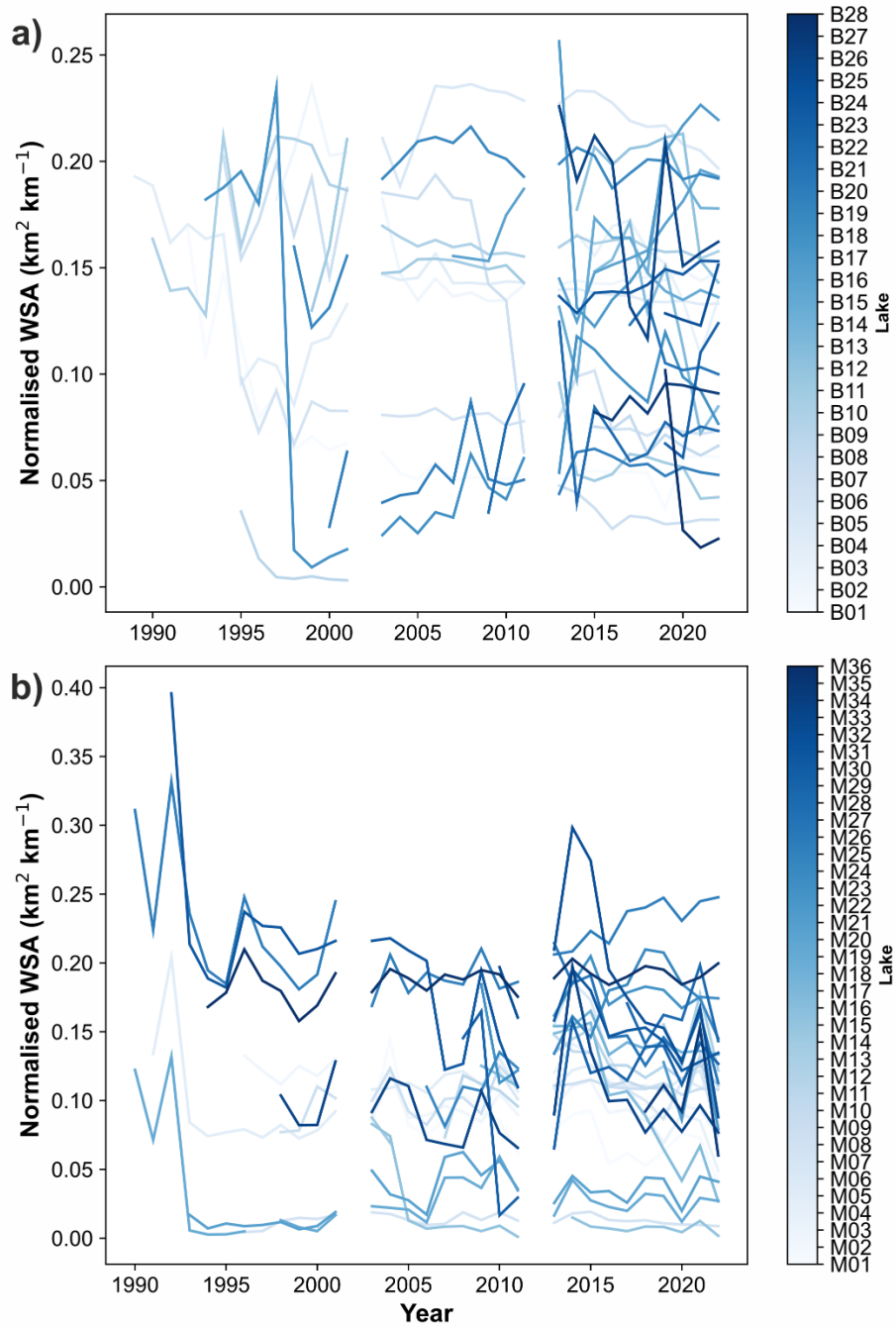
Figure 7. Interannual variations of normalised lake water surface area (WSA). a) Temporal transects of WSA variations on the Beni for each lake (01-28). b) Temporal transects of WSA for lakes on the Mamore (01-36). Transects are shaded by lake distance downstream, with darker shades being indicative of lakes situated further downstream. Transect length aligns with the temporal record of measurements. Images were unavailable for 2002 and 2012.
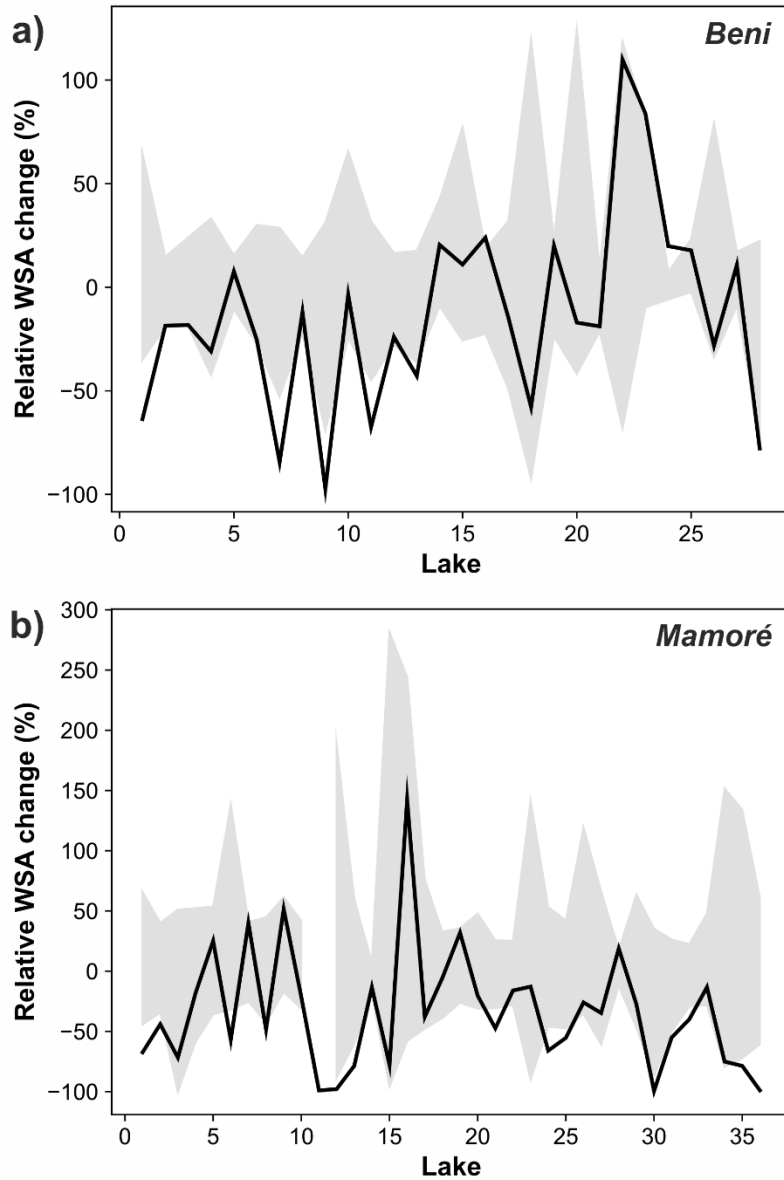
Figure 8. Relative water surface area changes for the a) Beni and b) Mamore. Long-term WSA changes measured between the first and final image on record for each lake is displayed by the solid black line. The grey shaded region indicates the range of WSA measurements for each lake measured from annual imagery over the full lifetime of the lakes. Some lakes display interannual changes in WSA that exceed the long-term changes.
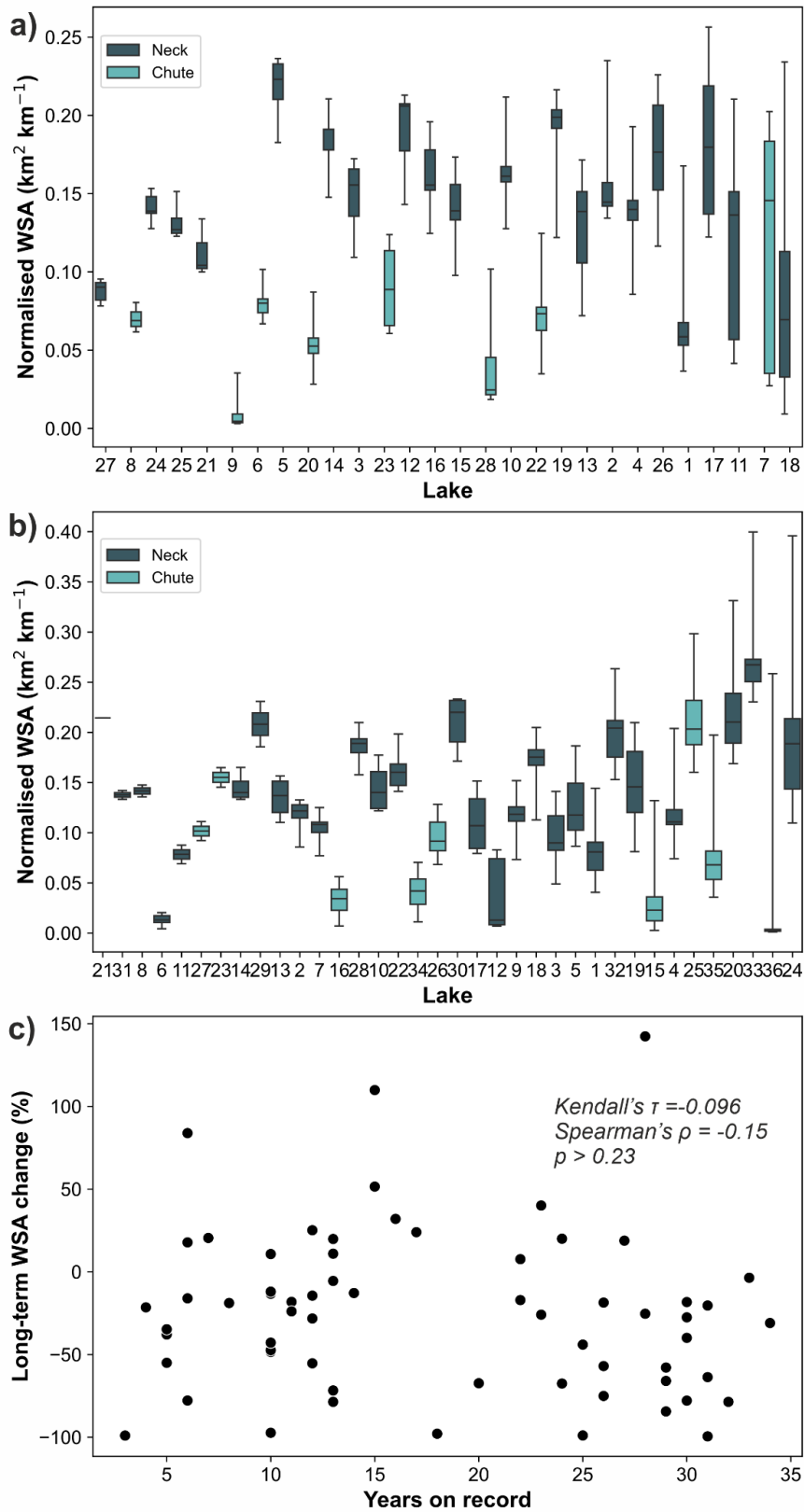
Figure 9. WSA distributions through time. a) WSA distributions for each lake on the Beni. b) WSA distributions for each lake on the Mamore. Boxes represent the interquartile range of measurements, with the central line indicating the median WSA measurement of each distribution. Bars indicate the full range of measurements for each distribution. Boxes are

symbolised according to the lake type (neck or chute) as displayed in the legend. Boxes are ordered in ascending range order, while lake numbers increase with distance downstream. c) Relative long-term WSA changes (those measured between the first and final images on record) ordered by the number of years on record. The results of statistical tests (Kendall's Tau, τ; and Spearman's rank, ρ, are displayed with associated p-value.
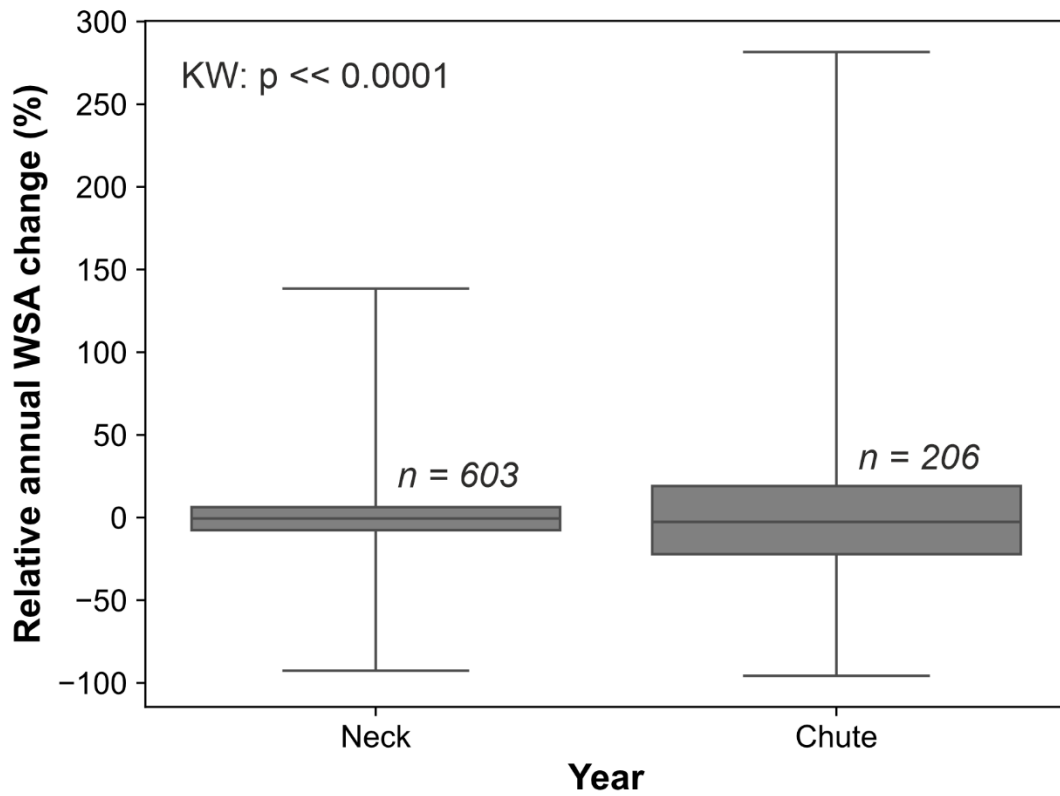
Figure 10. Distribution of relative annual WSA changes for different lake types. Boxes represent the interquartile range, with median value represented by the line within each box. The bars indicate the full range of measurements for each lake type. The p-value associated with a Kruskal-Wallis test for similarity is indicated along with associated n values for each dataset.
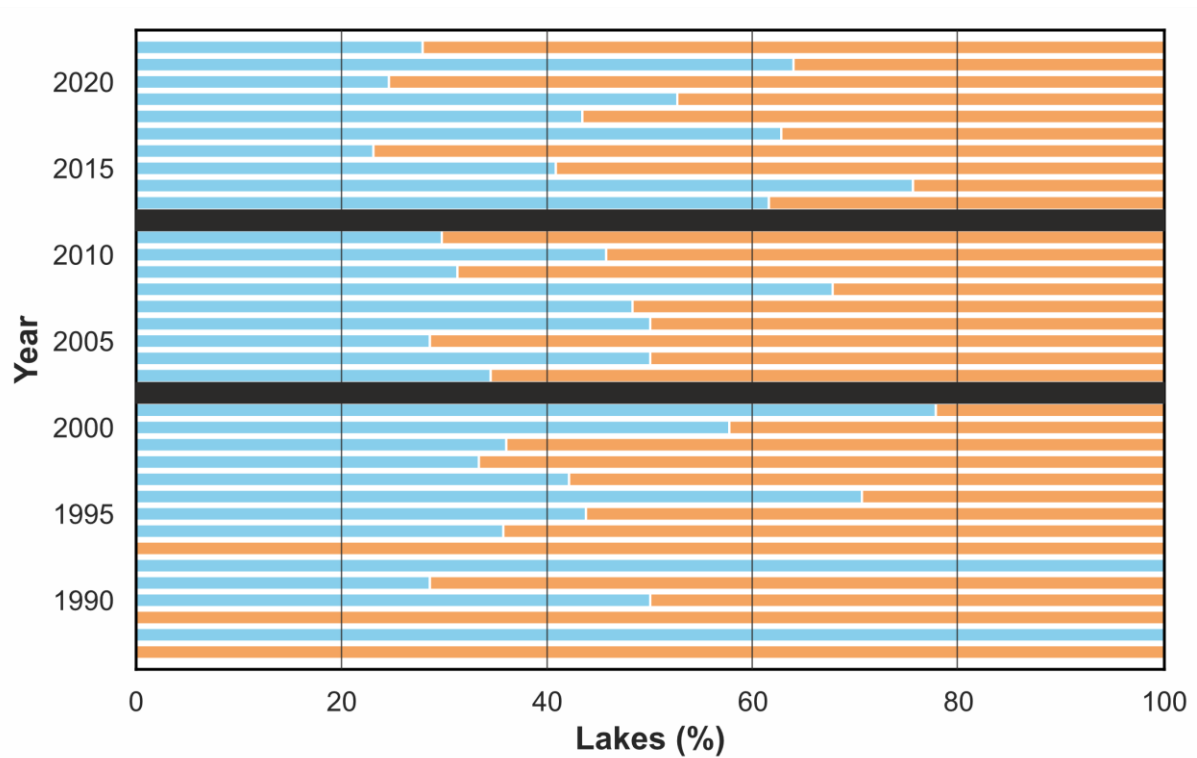
Figure 11. Annual comparisons of changes in lake behaviour. The percentage of lakes that increased (red) or decreased (blue) in size for each year (Lakes %) was used to establish catchment-scale changes in hydrological behaviour. Black boxes are indicative of data gaps for 2002 and 2012.
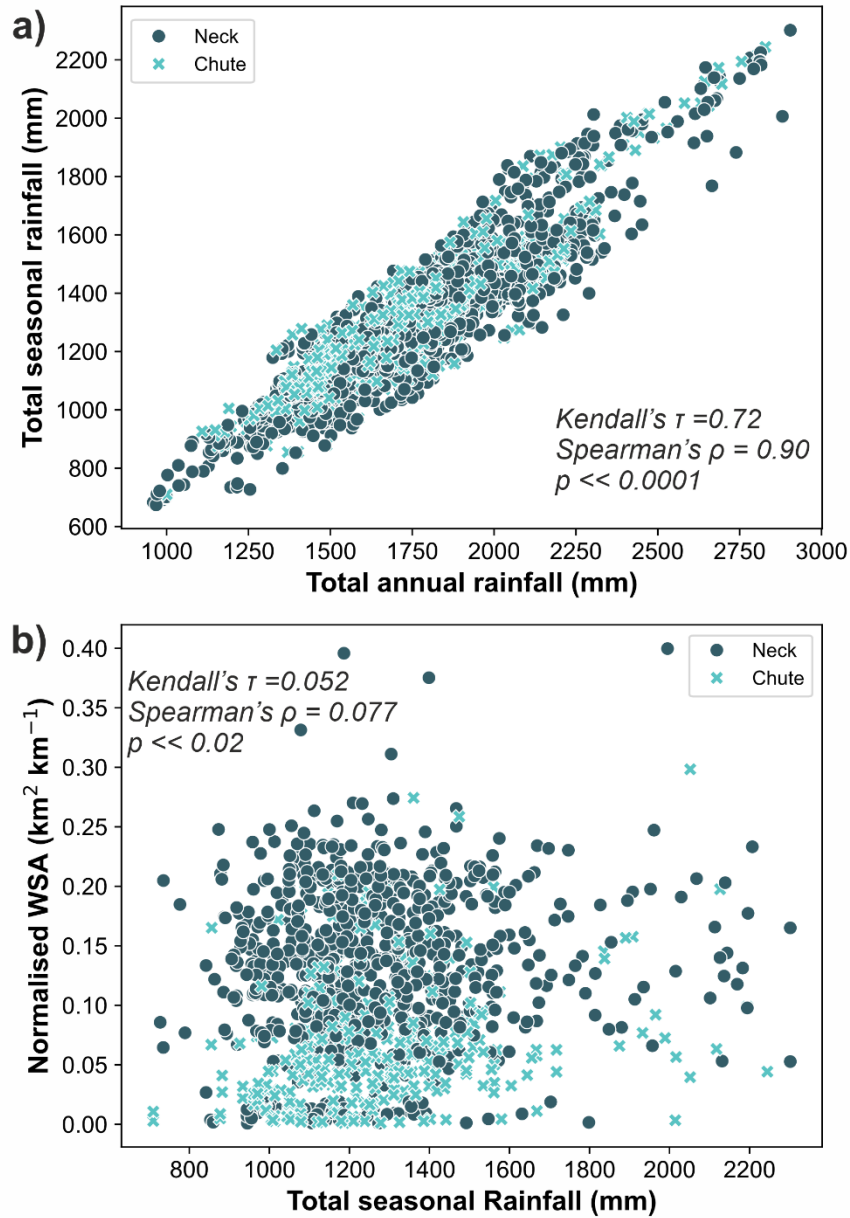
Figure 12. Precipitation patterns a) Total annual rainfall is predominantly controlled by total seasonal rainfall. Each measurement was collected once a year from within the boundary of the lakes. b) The response of lake WSAs to total seasonal rainfall for all lakes on record. Data points are symbolised according to the lake type over which measurements were taken. The statistical results from Kendall's Tau and Spearman's rank test and associated p-values are displayed.
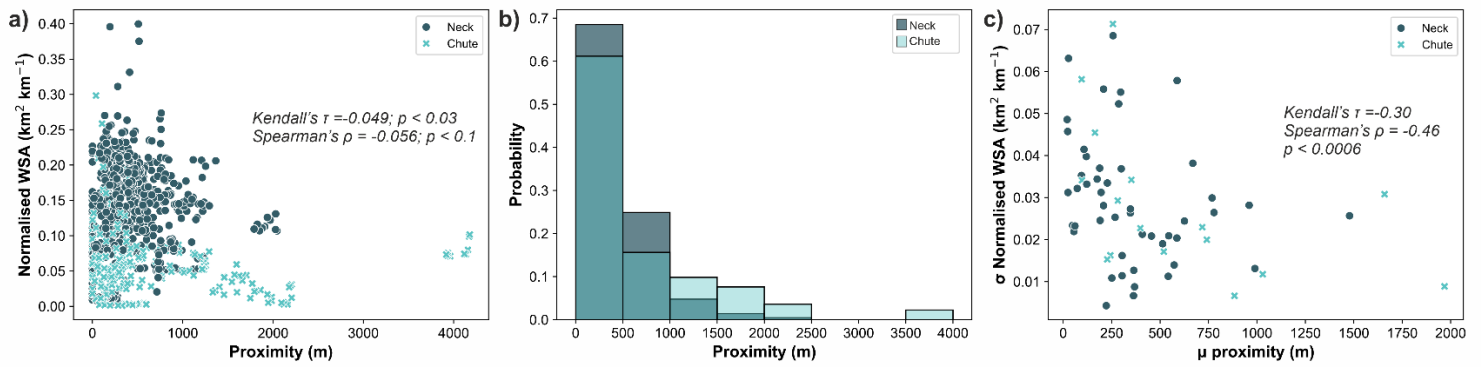
Figure 13. Relationships between WSA and channel proximity. a) WSA variations with respect to channel proximity. All lake WSA measurements and proximity to the mainstem for each lake and timestep on record. b) Histogram of WSA measurements for binned proximities. Each bin was 500 m in size and the WSA distribution was normalised by the total number of samples in each class (neck or chute). Bin size was arbitrarily scaled according to observations of channel proximity for the dataset. Where neck and chute lake populations overlap, bar symbology converges. c) Relationship between the standard deviation of lake WSAs (σ) and average proximity of each lake to the active channel (μ). These values were computed to remove temporal variability from the measurements of each variable. The statistical results of Kendall's Tau and Spearman's rank are displayed with associated p-values. Points and bars are symbolised by lake type as described by the legends.
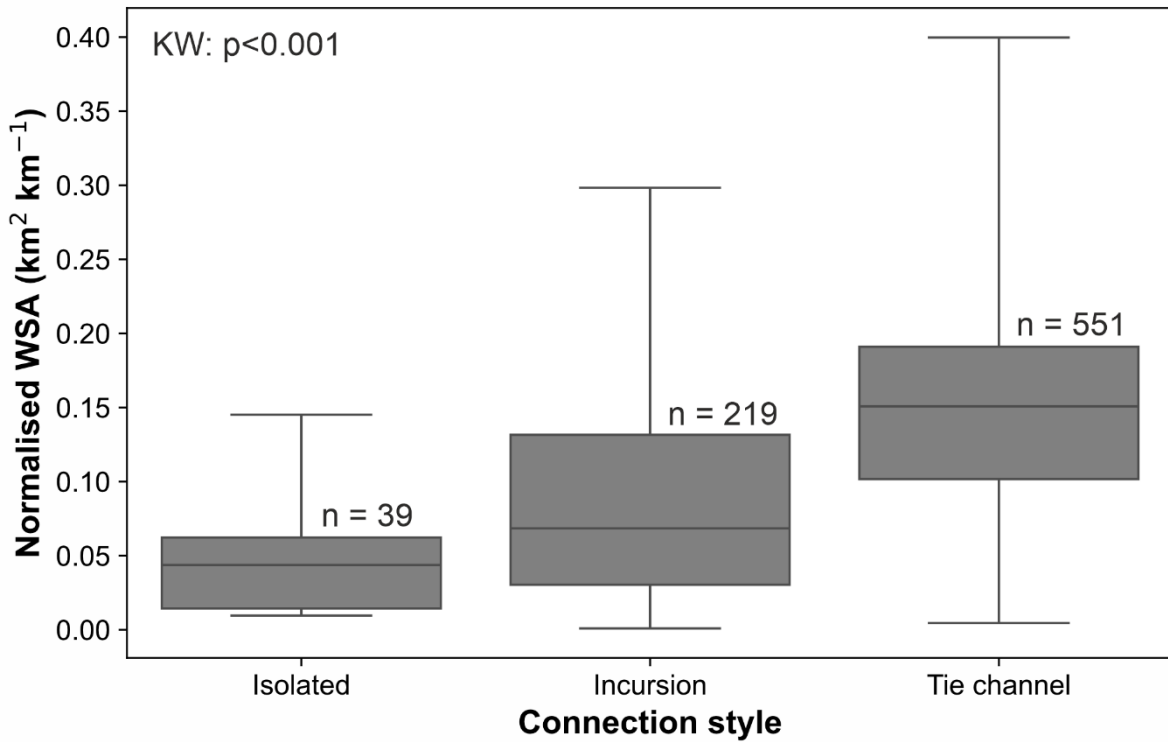
Figure 14. WSA distributions for different lake connection styles. Boxes represent the interquartile range of each distribution with the median represented by the line contained within each box. Bars describe the range of measurements for each connection type. The total number of measurements within each population is displayed above the boxes. The Kruskal-Wallis confidence value is displayed.